Clim. Past, 8, 1257–1285, 2012
www.clim-past.net/8/1257/2012/
doi:10.5194/cp-8-1257-2012

Climate of the Past

The relative roles of CO_2 and palaeogeography in determining late Miocene climate: results from a terrestrial model-data comparison

C. D. Bradshaw[1], D. J. Lunt[1], R. Flecker[1], U. Salzmann[2], M. J. Pound[2,3,4], A. M. Haywood[3], and J. T. Eronen[5,6]

[1]Bristol Research Initiative for the Dynamic Global Environment (BRIDGE), School of Geographical Sciences, University of Bristol, University Road, Bristol, BS8 1SS, UK
[2]School of the Built and Natural Environment, Northumbria University, Newcastle upon Tyne, NE1 8ST, UK
[3]School of Earth and Environment, University of Leeds, Leeds, LS2 9JT, UK
[4]British Geological Survey, Kingsley Dunham Centre, Keyworth, Nottingham, NG12 5GG,UK
[5]Department of Geosciences and Geography, P.O. Box 64, 00014, University of Helsinki, Finland
[6]Biodiversity and Climate Research Centre LOEWE BiK-F, Senckenberganlage 25, 60325 Frankfurt am Main, Germany

Correspondence to: C. D. Bradshaw (c.bradshaw@bristol.ac.uk)

Received: 23 February 2012 – Published in Clim. Past Discuss.: 9 March 2012
Revised: 7 July 2012 – Accepted: 9 July 2012 – Published: 16 August 2012

Abstract. The late Miocene palaeorecord provides evidence for a warmer and wetter climate than that of today, and there is uncertainty in the palaeo-CO_2 record of at least 200 ppm. We present results from fully coupled atmosphere-ocean-vegetation simulations for the late Miocene that examine the relative roles of palaeogeography (topography and ice sheet geometry) and CO_2 concentration in the determination of late Miocene climate through comprehensive terrestrial model–data comparisons. Assuming that these data accurately reflect the late Miocene climate, and that the late Miocene palaeogeographic reconstruction used in the model is robust, then results indicate that:

1. Both palaeogeography and atmospheric CO_2 contribute to the proxy-derived precipitation differences between the late Miocene and modern reference climates. However these contributions exibit synergy and so do not add linearly.

2. The vast majority of the proxy-derived temperature differences between the late Miocene and modern reference climates can only be accounted for if we assume a palaeo-CO_2 concentration towards the higher end of the range of estimates.

1 Introduction

The terrestrial palaeorecord contains evidence that the late Miocene (11.61–5.33 Ma; Gradstein et al., 2004; Hilgen et al., 2005) climate was, in many regions, much warmer and/or wetter than today (e.g. Pound et al., 2011, 2012). For example, warm temperate forests thrived in what is now the Circumboreal Region (Worobiec and Lesiak, 1998; Denk et al., 2005), and grasslands existed in modern desert regions (e.g. the Arabian peninsula, Kingston and Hill, 1999; the Sahara Desert, Vignaud et al., 2002). Moreover, although it is widely suggested that a large-scale Antarctic ice sheet has existed throughout the late Miocene (e.g. Shackleton and Kennett, 1975; Lewis et al., 2008), Northern Hemisphere glaciation is thought to have been limited (Moran et al., 2006; Kamikuri et al., 2007).

The late Miocene is also a period in which significant tectonic reorganisation occurred, including major tectonic uplift of the Himalayas (Harrison et al., 1992; Molnar et al., 1993; Rowley and Currie, 2006; Fang et al., 2005), the Andes (Gregory-Wodzicki, 2002; Garzione et al., 2008), the North American Rockies (Morgan and Swanberg, 1985), the East African Plateaus (Saggerson and Baker, 1965; Yemane et al., 1985), and the Alps (Spiegel et al., 2001; Kuhlemann, 2007). Significant differences existed in the oceans too, e.g. there is evidence for an open Panama gateway between the Atlantic and Pacific Oceans (Keigwin, 1982; Duque-Caro, 1990) and

an unrestricted Indonesian seaway between the Pacific and Indian Oceans (van Andel et al., 1975; Edwards, 1975; Kennett et al., 1985; Cane and Molnar, 2001) during the late Miocene.

Modelling studies have shown that late Miocene-like differences in palaeogeography and ice sheet extents are likely to have resulted in large changes to both atmospheric and oceanic circulation compared to the present day, e.g. Andes uplift (Takahashi and Battisti, 2007); Rockies uplift (Seager et al., 2002; Foster et al., 2010); uplift of the Tibetan Plateau (Ramstein et al., 1997; Lunt et al., 2010; Zhang et al., 2007a, b; Ruddiman et al., 1997; Kutzbach and Behling, 2004); Northern Hemispheric glaciation (Crowley and Baum, 1995; Lunt et al., 2004; Tonazzio et al., 2004); Panama gateway closure (Lohmann et al., 2006; Nisancioglu et al., 2003; Schneider and Schmittner, 2006; Lunt et al., 2008b); and closure of the Paratethys (Ramstein et al., 1997; Zhang et al., 2011). It is therefore reasonable to expect that the combination of all of these changes would result in a climate that was significantly different from that which we experience today, and this is supported by general circulation model (GCM) simulations for the late Miocene (e.g. Steppuhn et al., 2006; Gladstone et al., 2007; Lunt et al., 2008a; Micheels et al., 2011; Knorr et al., 2011). However, in order to evaluate the simulated late Miocene climate from a GCM, it is necessary to make quantitative comparisons with the palaeorecord.

Palaeo-CO_2 reconstructions suggest low concentrations in the atmosphere throughout the late Miocene, as shown in Fig. 1. Previous climate modelling has generally struggled to simulate the warm conditions inferred from the palaeorecord when imposing relatively low CO_2 concentrations in the models (e.g. Steppuhn et al., 2006; Micheels et al., 2007); although, a recent study which also included prescribed vegetation has met with some success, highlighting the importance of vegetation (Knorr et al., 2011). For computational reasons, most of the late Miocene modelling to date has not been carried out with a coupled atmosphere–ocean climate model, and recent work has highlighted the disparity between the results obtained from atmosphere-only or atmosphere–slab ocean models and coupled atmosphere–ocean models capable of incorporating important ocean circulation feedbacks (Micheels et al., 2011; Knorr et al., 2011). This is particularly important for simulating the late Miocene, since major reorganisation of Atlantic, Pacific and Indian Ocean circulation patterns occurred at this time (Collins et al., 1996; Kennett et al., 1985; Duque-Caro, 1990; Kameo and Sato, 2000; Cane and Molnar, 2001). Many of the most advanced GCMs now incorporate a dynamic land surface component which both responds and feedbacks to the atmospheric state, therefore allowing a more stringent test of the GCM than using a fixed late Miocene vegetation reconstruction.

These lines of evidence – warm/wet late Miocene climate, uncertain CO_2, significant tectonic uplift and ice sheet change – demand the question, "Can modelling inform what the likely relative roles of palaeogeographic changes and CO_2 concentrations are in determining late Miocene climate?" Here, we present the model results from a fully coupled atmosphere–ocean–vegetation GCM for the late Miocene, and compare our simulations with a synthesis of available climate proxies from the terrestrial realm. Most marine proxy data available for the late Miocene comes from the $\delta^{18}O_c$ of foraminifera, much of which has not been converted to palaeotemperature estimates. Furthermore, the treatment of the uncertainties associated with that data, such as $\delta^{18}O_{sw}$ reconstruction, depth habitat and seasonality considerations, and preservation, requires in-depth discussion which is outside the scope of this manuscript. Consequently, although we do show and discuss near-surface oceanographic differences between our late Miocene and modern control simulations, these differences will be described in more depth and compared with data in a forthcoming paper (Bradshaw et al., 2012).

As the timing and magnitude of the tectonic changes during the late Miocene are uncertain, GCM simulations for this period are representative of a large timeslab. However, this allows us to examine the impact of large changes in the palaeogeography and to assemble as large an amount of palaeodata as possible. We therefore examine the compiled palaeodata for any marked differences in the climate between the Tortonian (11.61–7.25 Ma) and the Messinian (7.25–5.33 Ma) of the late Miocene and compare the model simulations to those sub-datasets separately.

2 Data and model descriptions

In this section we describe the terrestrial palaeodata and the GCM that has been used, and discuss some of the uncertainties that are inherent in both.

2.1 Description of the quantitative late Miocene palaeodata

The palaeorecord of the late Miocene is sparse in comparison with more recent periods such as the Last Glacial Maximum (Farrera et al., 1999). We have compiled a total of 1030 terrestrial climate reconstructions from the literature for the climatic variables of mean annual temperature (MAT), mean annual precipitation (MAP), mean temperature of the coldest month (CMT) and mean temperature of the warmest month (WMT). We include in our database those data whose age uncertainty overlaps with our criteria for the late Miocene (5.33–11.61 Ma), see Appendix A for more information. As comparison is made to the dataset separately for the Messinian and the Tortonian stages, any data that had age uncertainty placing it between the two stages was duplicated, one datapoint residing in each stage. The total number of datapoints considered therefore increased to 1166.

The data synthesis largely consists of the data from the NECLIME database (Bruch et al., 2007; Utescher et al.,

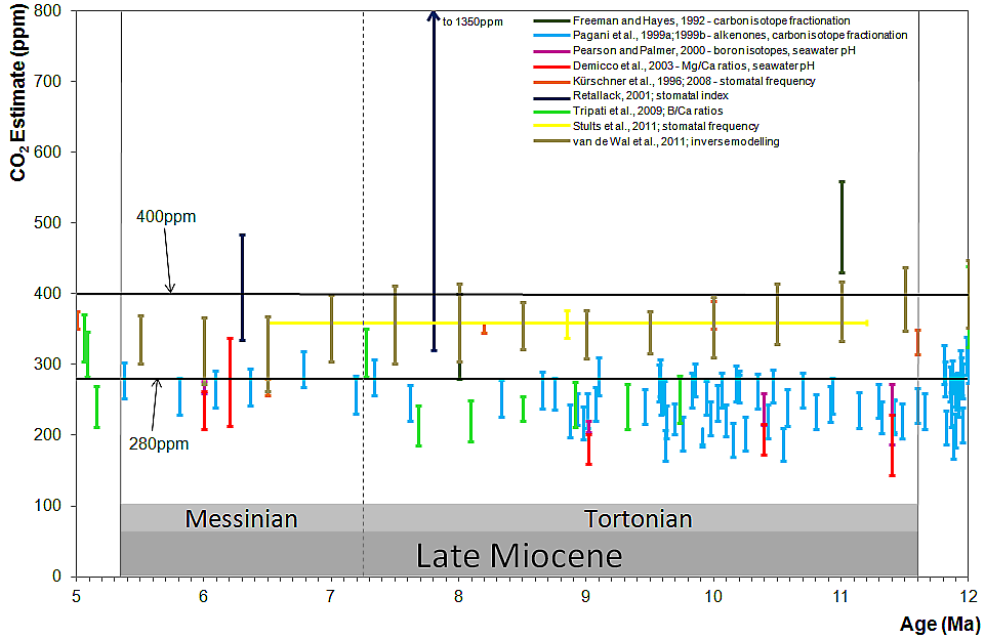

Fig. 1. Atmospheric CO_2 reconstructions for the late Miocene.

2011) and the NOW Neogene Mammal Database (Eronen et al., 2010; Fortelius, 2012) but also includes data from a variety of other sources including the data synthesis of (Steppuhn et al., 2007), as detailed in the Supplement. These reconstructions are derived from microfauna, macrofauna, microflora and macroflora proxies using a variety of different reconstruction methods, including the co-existence approach (Mosbrugger and Utescher, 1997), the climatic amplitude method (Fauquette et al., 2006), nearest living relative methods (Wolfe, 1993; Spicer, 2007; Spicer et al., 2009), species characteristic approaches (Eronen et al., 2010; Jacobs and Deino, 1996), and species composition approaches (Montuire et al., 2006; Bohme et al., 2008; van Dam, 2006). A discussion of the uncertainties in proxy reconstructions is given in Appendix A and all of these terrestrial data are provided in the Supplement. Comparison is also made to the biome reconstruction datasets of Pound et al. (2011, 2012).

2.2 Description of the modern reference climate (modern potential natural climate)

For the purpose of this study, we are interested in the late Miocene climate because we wish to understand how and why it was different from today. In terms of understanding these differences, we are only interested in the changes that occur under natural forcing (a modern potential natural climate); however, the modern instrumental record contains both natural and anthropogenic forcing. In order to make an estimate of the extent of anthropogenic influence on the modern instrumental record (IR_{20thC}), we derive grid-based correction factors using the anomaly between the "preindustrial" simulations ($Model_{preind}$) and the "20th century" simulations ($Model_{20thC}$) of the CMIP-4 GCM ensemble (IPCC, 2007), as detailed in Eq. (1). Through application of the correction factors, it is assumed that the modern instrumental record is a suitable proxy for the potential natural climate state.

$$\text{Modern potential natural climate} = IR_{20thC} - \left(\frac{1}{n}\sum_{i=1}^{n} Model_{20thC} - Model_{preind}\right) \quad (1)$$

The modern instrumental record used is the CRU-TS 3.0 Climate Database (Mitchell and Jones, 2005), an interpolation of mean monthly surface weather station data to a 0.5×0.5 degree grid, spanning the period 1900–2006. The modern climate estimates for temperature and precipitation at any grid point will be least certain in areas of largest interpolation where no weather stations exist, but in other areas there is uncertainty in the records too due to limited temporal operation of some stations, station movement, urbanisation and other land-use changes. The observational datasets are at a higher spatial resolution than the HadCM3L model; therefore when aggregating the observations to the HadCM3L model resolution, the minimum and maximum values within each grid box are retained in order to account for within-grid box uncertainty.

2.3 Description of the models

2.3.1 HadCM3L GCM

The Hadley Centre Coupled Model, version 3 (HadCM3) is a fully coupled atmosphere–ocean general circulation model

comprising the atmospheric model HadAM3 (resolution 2.5° latitude by 3.75° longitude) and the ocean model HadOM3 (resolution 1.25° latitude by 1.25° longitude) (Gordon et al., 2000). It is computationally demanding to run HadCM3 simulations to equilibrium, so we use a reduced ocean resolution version, HadCM3L (resolution 2.5° latitude by 3.75° longitude) (Cox et al., 2000). In order to run the model without the use of flux corrections, we removed the two grid cells representing Iceland (Jones, 2003). Full details of the model are given in Appendix B, Sect. 1.1.

2.3.2 TRIFFID and BIOME4 vegetation models

The dynamic global vegetation model coupled to HadCM3L is TRIFFID (Top-down Representation of Interactive Foliage and Flora Including Dynamics), a full description of which is given in Cox (2001) and Hughes et al. (2004). Refer to Appendix B, Sect. 2.1 for more details about the TRIFFID model and its uncertainties.

In order to make model–data comparisons with a recently published biome reconstruction dataset for the late Miocene (Pound et al., 2011, 2012), the HadCM3L model climatologies are used to drive the BIOME4 vegetation model offline (Kaplan, 2001; Kaplan et al., 2003). The 28 different vegetation classes used by Pound et al. (2011, 2012) match the vegetation classifications of the BIOME4 model, which has successfully been used for previous pre-Quaternary vegetation model–data comparisons (e.g. Salzmann et al., 2009). See Appendix B, Sect. 3.1 for a discussion of the uncertainties in the BIOME4 model.

2.3.3 Model uncertainties

A discussion of model uncertainties is given in Appendix B. The GCM simulations were integrated over 2100 model years. Particular attention is given to the question of equilibrium in the climate system, particularly for the deep ocean as it has been shown that the global mean air temperature may not be a good indicator of model equilibrium (Brandefelt and Otto-Bliesner, 2009). The trends in the global mean ocean temperature are very small for the late Miocene simulations ($< 8 \times 10^{-4}$ °C century^{-1}) and our control simulation (5×10^{-4} °C century^{-1}), although it is not possible to rule out some remaining disequilibrium. The analysis in this paper is carried out using the climatological means of the last 50 yr of the simulations after the TRIFFID dynamic mode was used for 100 yr to ensure full consideration of interannual variability in the vegetation component.

3 Experiment design

3.1 Model setup

For the late Miocene, the palaeogeography (including ice sheet geometry) derived by Markwick (2007) is used, which is representative of the timeslab 11.6 to 5.3 Ma. The length of this palaeogeographic timeslab is necessarily long due to difficulties associated with the poorly constrained chronology and age estimate uncertainty for the various tectonic and ice sheet changes (Markwick and Valdes, 2004).

The orography, ice sheet configuration and continental positions assumed for the model simulations are shown in Fig. 2, and are discussed in detail in Appendices B and C, together with a discussion of the associated uncertainties in the late Miocene boundary conditions.

For the modern control simulation (hereafter referred to as CTRL), we use the standard UK Meteorological Office configuration for the model boundary conditions as described in Appendix C. The late Miocene boundary conditions significantly reduce the elevations of most of the highest regions as compared to CTRL, and ice sheet extents and thicknesses are also altered. Notable changes to the land–sea mask for the late Miocene include the open Panama gateway, the open Indonesian seaway, the closed Bering Strait, the extension of Eurasia into the Arctic and the more southerly position of Australia.

We carried out two late Miocene simulations with two different values of atmospheric CO_2 concentration. Firstly, a value of 280 ppm was used, the same as CTRL; the difference in climate between these two simulations indicates the role of the palaeogeographic changes that we have made on the simulated climate. Secondly, a value of 400 ppm was used in order to test the sensitivity of the results to uncertainties in the CO_2 concentration; the difference between the 400 ppm simulation and the 280 ppm simulation indicates the role of CO_2 in determining the simulated late Miocene climate. These values are well within the range of uncertainty of late Miocene CO_2 concentrations based on the available proxy data, shown in Fig. 1. The late Miocene simulation with a 280 ppm CO_2 concentration is hereafter referred to as LM280, and the simulation with a CO_2 concentration of 400 ppm is referred to as LM400. We test the non-linearity of our results with an additional simulation which is identical to the CTRL simulation except that an atmospheric CO_2 concentration of 400 ppm is used.

The model output temperature and precipitation fields are provided as Supplement. Further climate variables that may be of interest can be obtained from the BRIDGE resources webpage, http://www.bridge.bris.ac.uk/resources/simulations.

3.2 Model–data comparison methodology

There are many difficulties associated with developing a methodology for a model–data comparison and in the interpretation of any results. We have considered uncertainties associated with model and data reconstructions that are often overlooked. These include uncertainties associated with the reference climatologies, poor temporal constraint leading

Table 1. Calibration errors for climate reconstructions of proxy data.

Method	MAT (°C)	MAP (mm a^{-1})	CMT (°C)	WMT (°C)	Reference
Climatic amplitude approach	3.4	257	5.5	2.9	Fauquette et al. (1998)
Coexistence approach	2	200	as MAT	as MAT	Mosbrugger and Utescher (1997); this study
Small mammal species composition		350–400			van Dam, 2006
Herpetofaunal composition		250–275			Bohme et al. (2008)
Mammal tooth crown height		388			Eronen et al. (2010)
CLAMP	1–3		1.5–3	1–4	Wolfe (1994); Teodorides et al. (2011)
Leaf morphology	1.98	57.97	3.55	2.92	Jacobs and Deino (1996)
Rodent species composition	0.004–4.8				Montuire et al. (2006)
Palaeosol analysis		141			Retallack et al. (2002a)
CLAMP multiple regression analysis	0.7	180			Gregory-Wodziscki (2000)
Physiognomic/morphology reconstructions	as CLAMP		as CLAMP	as CLAMP	this study
Nearest living relative, autecology	as Climatic amplitude approach	as Climatic amplitude approach	as Climatic amplitude approach	as Climatic amplitude approach	this study

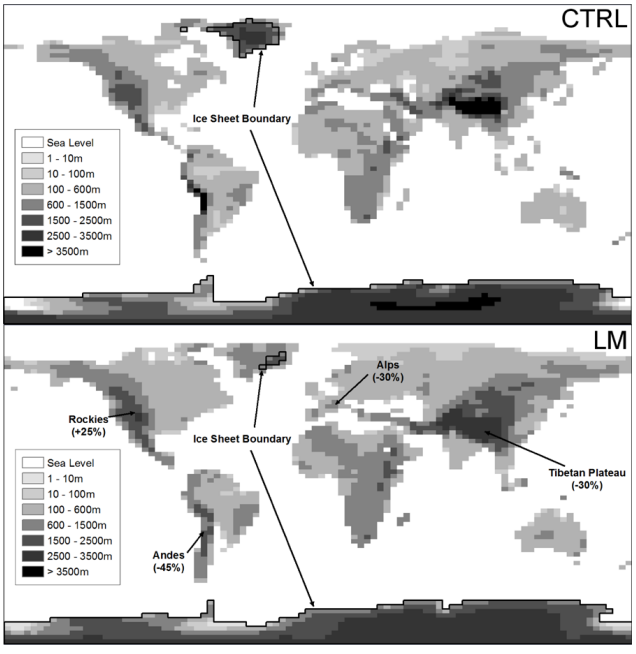

Fig. 2. Model orographic and ice sheet configurations for the preindustrial (CTRL) and the late Miocene (LM). The LM panel shows the percentage differences in high topography between CTRL and LM.

to data location uncertainty, data transportation issues and palaeorotation uncertainty.

The methodology for estimating error ranges for each data record is as follows. First, we estimate the modern calibration error for each proxy type, if this is not already given in the original source, by assuming the same calibration error as the next most similar proxy reconstruction method (for example, by assuming that the physiognomic/morphology reconstructions have the same uncertainty as defined for CLAMP; see Table 1 for full details).

Secondly, we translate the individual proxy data locations back to their estimated palaeolocations as dictated by their age control, with the uncertainty in age resulting in a number of possible locations for each data point. We use the same palaeorotation as Markwick (2007) to ensure consistency with the late Miocene palaeogeography used in HadCM3L. As we do not include Iceland as land in our model, we exclude the Icelandic data from our analysis.

Thirdly, we consider it unreasonable to expect our climate model to be able to reconstruct the exact climate at a single grid cell given the model uncertainties outlined in Appendix B and because comparisons made between the BIOME4 model and maps of potential natural vegetation have shown that greater reliance should be placed on broad-scale patterns rather than individual grid cells (Prentice et al., 1992). We therefore assume that all grid cells adjacent to the cell containing palaeodata could potentially be consistent with that data. Taking this approach to the model–data comparisons also allows for uncertainties in the true location of the data due to either transportation or incorrect assumptions in the palaeorotations applied.

Because HadCM3L does not completely reproduce the modern reference climatology in the CTRL simulation, it is assumed that the relative differences simulated by the model are more robust than the absolute values, and results are presented as the anomaly between the late Miocene simulations and the modern control simulation. When comparisons are made between the model results and the palaeorecord, bias corrections are applied to the simulation results (the anomalies between the modern control simulation and the modern reference climate). As the CTRL simulation is designed to represent the modern potential natural climate and not the climate of the 20th century, we are unable to use the ideal bias correction factors given in Eq. (2):

$$\mathrm{Model}_{\mathrm{HadCM3L}} = \mathrm{Model}_{\mathrm{HadCM3L}} + (\mathrm{Observations}_{20\mathrm{thC}} - \mathrm{Model}_{\mathrm{HadCM3L20thC}}) \quad (2)$$

Therefore, the modern potential climate estimates from Eq. (1) are used, as detailed in Eq. (3):

$$\text{Model}_{\text{HadCM3L}} = \text{Model}_{\text{HadCM3L}} + (\text{Modern potential natural climate} - \text{CTRL}) \quad (3)$$

Where bias corrections have been applied to the model simulations, these are denoted by the subscript "c", e.g. LM280c. When these corrections are applied to the modern control simulation CTRL, Eq. (3) reduces to:

$$\text{CTRLc} = \text{Modern potential natural climate.} \quad (4)$$

Whilst it is possible to make bias corrections to the climatology, we are unable to do the same for TRIFFID modelled vegetation cover because of the interactive coupling within the climate model. The standard anomaly method is, however, applied when forcing the BIOME4 model (e.g. Haxeltine and Prentice, 1996; Texier et al., 1997) by applying a correction factor equal to the anomaly between the CTRL model climate and the modern climate; although, it should be noted that this correction is based on the modern instrumental record and does not include our estimates of uncertainty of that record for a modern potential natural climate. In order to simplify the model–data comparison, the 28 biomes of the BIOME4 model are combined into 9 megabiomes: tropical forest, temperate forest, warm-temperate forest, grassland and dry shrubland, savannah and dry woodland, tundra, boreal forest, desert and land ice.

To reflect the uncertainties in the data reconstructions and model results, both are treated as a range of possible values rather than the mean of possible values. The term "overlap" is defined as consistency between model and data if their uncertainty ranges overlap (see Fig. 3a). Overlap between model and data does not necessarily imply "good" agreement because the uncertainty ranges may be large, but rather that where model and data do overlap, it is not possible to determine that they are different. In the figures and discussion that follow, the differences between model and data uncertainties are defined as the minimum possible difference given the range of possible values for both; if the true values for each were at the extremes of their respective uncertainties, then the differences between the two would be much larger (see Fig. 3b).

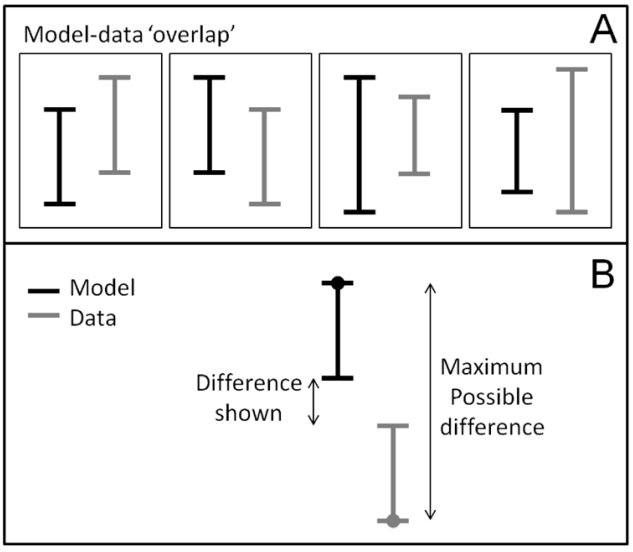

Fig. 3. Model–data comparison definitions. Panel **(A)** shows the definition for "overlap" used in the model–data comparison: all four instances shown are considered as an overlap. Panel **(B)** shows that although we define model–data mismatch as the minimum possible distance to overlap, the maximum possible differences could be much greater if the true values for both the model and the data were to lie at the extremes of the uncertainty ranges.

4 Description of the simulated late Miocene climate

Here, model results are described in terms of anomalies – the difference between the late Miocene (LM280 or LM400) and the modern (CTRL) climates. We also conduct a model–model comparison of the present work with respect to previous Miocene GCM simulations, although direct comparison is difficult where different palaeogeographies, model complexity and ocean model setup have been used. Comparison between results from different vegetation models is even more difficult because of the different plant functional types (PFTs) and biome classification systems used. The late Miocene simulations have been used to drive the interactive vegetation model TRIFFID, which is coupled to the climate in the GCM, but also offline to drive the BIOME4 model; therefore, it is possible to make some general comparisons between the results of the two vegetation models we have used.

4.1 Global

The annual and seasonal (DJF – December/January/February, JJA – June/July/August) mean air temperature and precipitation anomalies between our late Miocene and CTRL experiments are shown in Figs. 4a–c and 5a–c. The magnitudes of the global anomalies are modest for LM280-CTRL (the impact of changing palaeogeography alone), with the MAT only 0.3 °C higher and the MAP only 4.5 mm a^{-1} (0.4 %) higher. The Micheels et al. (2011) model results obtain a larger MAT difference of 1.5 °C between their same CO_2 Tortonian and control simulations. However, these results are not really comparable to ours because of the palaeogeographic differences between our studies and the fact that they used a prescribed late Miocene vegetation in their Tortonian simulations. It could also be that the influence of palaeogeographic change is dependent on the background CO_2 (e.g. Micheels et al., 2011 assume a CO_2 concentration of 360 ppmv for both simulations compared to our 280 ppmv). The magnitudes of the global anomalies

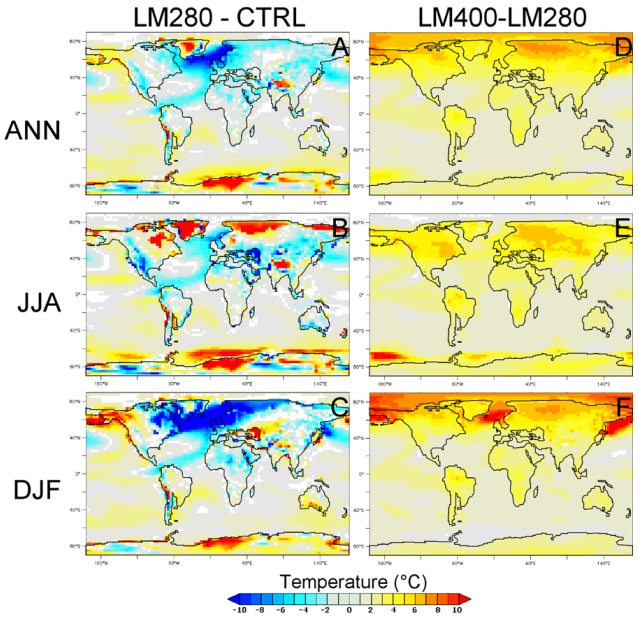

Fig. 4. Difference between the late Miocene and preindustrial simulations (LM280-CTRL, left side) and between the late Miocene CO_2 simulations (LM400-LM280, right side) for mean air temperature. Only significant differences are shown using a 95 % confidence interval Student's *t*-test; white areas are not significant.

are higher for LM400-CTRL (the impact of changing palaeogeography and CO_2 concentration), with the MAT 2.88 °C higher and the MAP 46.6 mm a^{-1} (4 %) higher.

4.2 Regional

Regions of palaeogeographic change in the late Miocene simulations, either due to ice removal or lower mountains, generally experience significant increases in temperature (Fig. 4a–c). These changes are consistent with the lapse rate cooling effect and have been found in other modelling studies of ice removal (Lunt et al., 2004; Tonazzio et al., 2004) and mountain uplift (Foster et al., 2010). However, since we have performed a number of palaeoenvironmental changes simultaneously, these simulations represent a combination of all of these changes.

4.2.1 High latitudes

Over Greenland we find a mean annual warming of the interior due to palaeogeographic change of more than 10 °C as shown in Fig. 4a, with a maximum warming of 8 °C and 21 °C for DJF and JJA, respectively (Fig. 4b–c). Lapse rate corrected temperature calculations reveal these temperatures to be ∼ 3–5 °C cooler than would be expected due solely to topographic lowering. In LM280, the DJF precipitation over most of Greenland is very low (< 0.5 mm day^{-1}; Fig. 5c) and the ice-free land surface remains largely snow-free, resulting in a lower land surface albedo for LM280 than CTRL in both DJF and JJA, consistent with the small imposed late Miocene Greenland ice sheet in the GCM (Fig. 2). A reduction in the albedo should also lead to warming of this region. Several modelling studies report warming across the whole of Greenland, and further afield, as a result of the complete melting of the Greenland ice sheet (Crowley and Baum, 1995; Tonazzio et al., 2004; Lunt et al., 2004), whereas our study shows large areas of cooling in the North Atlantic. This could be due to the impact of an open Panama gateway (e.g. Lunt et al., 2008b), differences in runoff from a less-glaciated Greenland and from the late Miocene Arctic Eurasian landmass, or it could also be caused by vegetation–climate feedback mechanisms, potentially affected by the high latitude cold bias in our GCM. Although there is little significant difference in the high latitude vegetation cover predicted by the TRIFFID model for the palaeogeographic changes we have made (Fig. 6a compared to Fig. 6b), there are large changes in vegetation predicted for the CO_2 increase (Fig. 6b compared to Fig. 6c). The unglaciated areas of Greenland and the high latitudes of North America and Eurasia are modelled as vegetated by TRIFFID with the dominant PFT being C3 grasses for LM280 (Fig. 6b), altering to shrub for LM400 (Fig. 6c). Figures 4f and 5f show that the largest climatic changes as a result of higher CO_2 are seen in the winter months of the high northern latitudes. Both vegetation models (TRIFFID and BIOME4) agree that the higher CO_2 LM400 simulation has more trees at the high northern latitudes, in Asia and in North America, than the lower CO_2 LM280 simulation, for which grasses are predicted.

The Antarctic orographic differences result in temperature anomalies between LM280 and CTRL that are broadly consistent with the lapse rate cooling effect, but opposite to the Greenland case in that the changes are slightly greater than lapse rate corrected temperature calculations suggest. The high southern latitudes are generally simulated as being significantly warmer and having significantly more precipitation in LM280 than CTRL, and these changes are more pronounced in JJA (Southern Hemisphere winter) than DJF (Southern Hemisphere summer). The Southern Ocean has significantly less sea ice in both LM280 and LM400 than in CTRL (not shown), and we infer that the reduction in the ice-albedo feedback mechanism amplifies the warming associated with topographic lowering.

4.2.2 Eurasia

The model results suggest that palaeogeographic changes alter the seasonality of the late Miocene climate of the southwestern European countries, which are generally simulated to be warmer (with some grid boxes up to 6 degrees warmer) and drier in the summer months (Figs. 4b and 5b), and cooler and wetter in the winter months (Figs. 4c and 5c) for LM280 compared to the CTRL. Conversely, a reduction in seasonal temperature range is seen in LM280 compared to CTRL in the region from the Paratethys across into

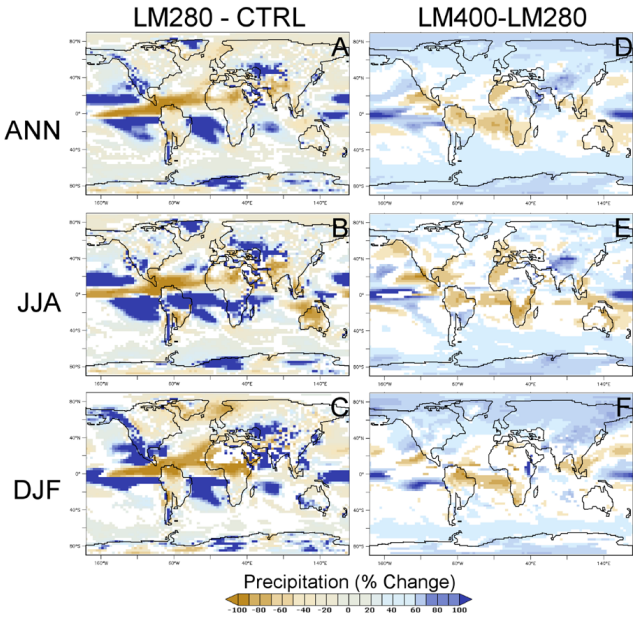

Fig. 5. Difference between the late Miocene and preindustrial simulations (LM280-CTRL, left side) and between the late Miocene CO_2 simulations (LM400-LM280, right side) for mean precipitation. Only significant differences are shown using a 95 % confidence interval Student's *t*-test; white areas are not significant.

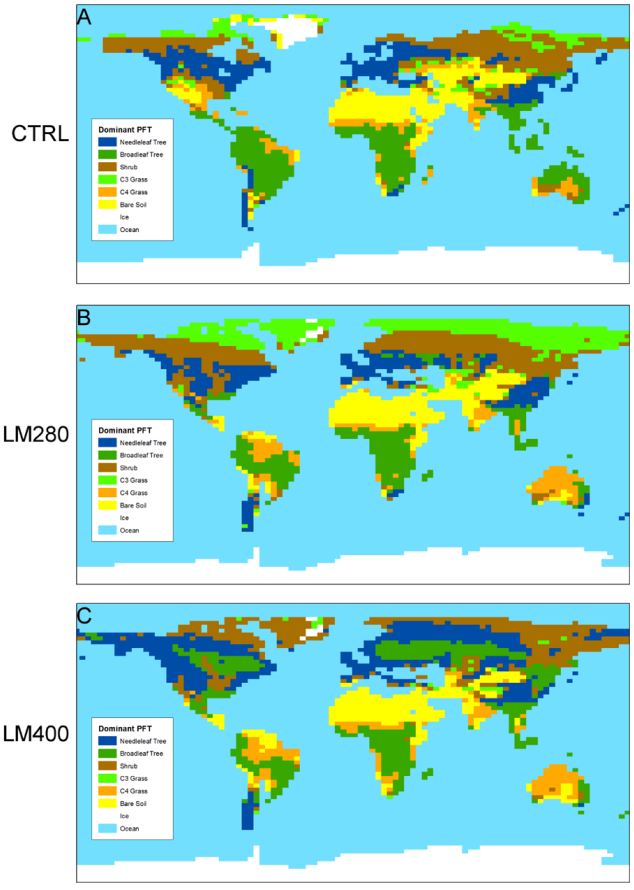

Fig. 6. Dominant PFTs of the late Miocene and preindustrial simulations, as predicted by the TRIFFID dynamic vegetation model.

central-eastern Asia, and both DJF and JJA are modelled as wetter in LM280 than in CTRL. These changes are consistent with simulations of the closure of the Paratethys (e.g. Ramstein et al., 1997) and with the evidence in this region for dynamic changes in vegetation and mammal communities across the late Miocene with the rise and fall of the Pikermian palaeobiome (see Eronen et al., 2009, and references therein). There is a shift in the distribution of modelled PFTs in Central Asia from a mix of shrubs, trees and grasses in LM280 to bare soil in CTRL, causing large changes in surface albedo (not shown). There are large differences in the predicted vegetation in this locality for LM400 compared to LM280, with the majority of Eurasia being forested under the LM400 scenario (Fig. 6c).

We calculate lapse rate corrected temperatures for this region and suggest that topographic changes in the Tibetan Plateau are largely responsible for the LM280 warming seen here in DJF. In JJA however, the temperatures are $\sim 3\,^{\circ}C$ cooler than lapse rate corrections would suggest. Our study indicates a decrease in JJA precipitation across the northern Indian Ocean and the Indian subcontinent, indicating a weakened monsoon, and this is consistent with many modelling studies (Ramstein et al., 1997; Steppuhn et al., 2006; Lunt et al., 2008a; Zhang et al., 2007a, b). However, the vegetation reconstructions for the Indian subcontinent are composed of tropical forests and savanna, which suggests an increase in precipitation relative to today (Pound et al., 2011, 2012). These reconstructions are consistent with some modelling studies (e.g. Lunt et al., 2008a; Micheels et al., 2011) which simulate large increases in precipitation in this region. It is not clear what the probable cause of these differences in our results for this region might be.

Away from the Tibetan Plateau, Southern Asia is cooler in LM280 than CTRL, in disagreement with many modelling uplift studies that suggest this region could have been $\sim 5\,^{\circ}C$ warmer with lower orography (Ruddiman et al., 1997; Kutzbach and Behling, 2004) and also in disagreement with other late Miocene climate simulations (Knorr et al., 2011; Micheels et al., 2011). We suggest that either the changes we have made to the Indonesian seaway may play an important role in the climate of Southern Asia, or that this region is very sensitive to other palaeoenvironmental differences. However, our modelled Southern Asia vegetation changes are generally consistent with other modelling work (Kutzbach and Behling, 2004; Lunt et al., 2010).

4.2.3 Americas

In northwestern America, there are cooler temperatures and an increase in precipitation simulated for LM280 compared to CTRL (Figs. 4 and 5). Correspondingly, the PFT

distribution changes from wooded vegetation in the late Miocene simulations to deserts in CTRL, and this result is robust to the CO_2 concentration assumed (Fig. 6). Alaska and northwest Canada are warmer and wetter in the late Miocene simulations than CTRL. Vegetation changes here are small if only palaeogeographic changes are considered (Fig. 6a and b), but much larger under a higher late Miocene CO_2 assumption (Fig. 6a and c).

Over Central America the late Miocene configuration simulates colder and drier air than CTRL, with a large reduction in JJA precipitation (Fig. 5). In this region C4 grasses and bare soil are simulated for the late Miocene, replaced by trees in CTRL, and this finding is robust to the CO_2 concentration assumed for the late Miocene (Fig. 6). Both vegetation models agree that in modern Central America, an open Panama gateway results in the desertification of the southern tip of North America and the northern tip of South America for both CO_2 concentration assumptions, and therefore we are confident that this vegetation change is due to the palaeogeographic changes made.

In South America, temperature changes between the late Miocene simulations and the CTRL are small, and those seen in Fig. 4c are generally associated with the differences in the land–sea mask of the two simulations. There is some warming in the region of Andean uplift for the late Miocene compared to CTRL. The largest climatic changes in this region though are for precipitation, which shows an increase in seasonality with wetter winters (JJA) and drier summers (DJF). Vegetation changes here are also notable (Fig. 6). The Patagonian region is simulated as dominated by the needleleaf tree PFT in LM280 and LM400, changing to desert in CTRL. The Amazon Rainforest is much reduced in our late Miocene simulations compared to CTRL, replaced by C4 grass and bare soil PFTs. As similar vegetation distributions occur in LM280 and LM400, we are confident that the vegetation changes are due to the palaeogeographic alterations made. There is very little difference in the vegetation predictions for the tropics between the two CO_2 scenarios by TRIFFID, however BIOME4 predicts quite large differences between the two CO_2 scenarios, such that the tropical forests of the lower CO_2 scenario are replaced by grasslands and dry shrublands; this trend is seen not only in South America, but also in Africa and in SE Asia.

4.2.4 Africa/Middle East

Widespread year-round reductions in precipitation, an increase in seasonality and the expansion of the Sahara Desert occurs in North Africa in the late Miocene simulations compared to CTRL (Figs. 4, 5 and 6). The presence of the Sahara Desert itself can contribute to cooling at high latitudes and the aridification/cooling of North Africa (Micheels et al., 2009b). Evidence of rooting systems in the Saharan region during the late Miocene suggests the presence of some vegetation (Duringer et al., 2007), but it is suggested that this vegetation was probably seasonal in nature, with the landscape alternating between being sand-covered and vegetated due to the presence of large lakes (Duringer et al., 2007; Vignaud et al., 2002). The large area of reduced precipitation that extends from the mid-Pacific Ocean into North Africa is in direct contrast to the Lunt et al. (2008a) study which showed large increases in precipitation in these regions. In the Micheels et al. (2007) work, the prescribed vegetation assumed in the Sahara (grasslands and savannahs) in their TORT simulations was responsible for up to 6 °C of warming and increases in precipitation in North Africa.

All of the areas predicted to be bare soil by TRIFFID are predicted to be slightly more vegetated by BIOME4.

4.2.5 Australia

Australia is drier in winter for the late Miocene simulations compared to CTRL; the band of increased precipitation for DJF, Fig. 5f, is most likely an artefact of the different land–sea masks in the two simulations. The palaeorecord provides evidence for the aridification of central Australia as a result of continental drift (Truswell, 1993; McGowran et al., 2004) which is perhaps consistent with our simulated precipitation results.

The TRIFFID model results clearly show vegetation changes as Australia shifts northwards between the late Miocene and CTRL simulations. In the late Miocene experiments, Australia is dominated by C4 grass and bare soil PFTs, largely replaced by the broadleaf tree PFT in the CTRL (Fig. 6). However, the interpretation of the TRIFFID results and analysis of the role of palaeogeography and CO_2 in this region are hampered by the inconsistencies between the vegetation modelled by TRIFFID and the modern Australian vegetation distribution.

5 Model–data comparison results and discussion

In this section we compare our simulations with the late Miocene terrestrial proxy data reconstructions (hereafter referred to as LMdata) to assess the extent to which solely changing the palaeogeography to that appropriate for the late Miocene results in a better consistency with this dataset, and to determine the sensitivity of those results to the uncertainty in the palaeo-CO_2 record.

We compare LMdata, categorised into the two stages of the Messinian and the Tortonian, with the climatologies of (a) the bias corrected CTRL simulation, equivalent to our modern potential climate estimates; (b) the bias corrected LM280 simulation; and (c) the bias corrected LM400 simulation. The extent to which comparison (b) is better than comparison (a) indicates the importance of palaeogeographic changes in determining late Miocene climate. The extent to which comparison (c) is better than comparison (b) indicates the

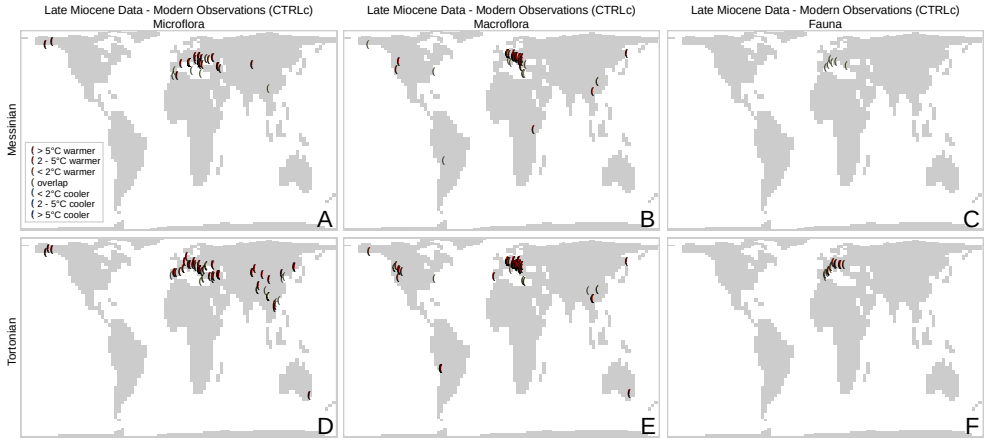

Fig. 7. Results from the model–data comparison for mean annual temperature, late Miocene data–modern potential natural climate estimates.

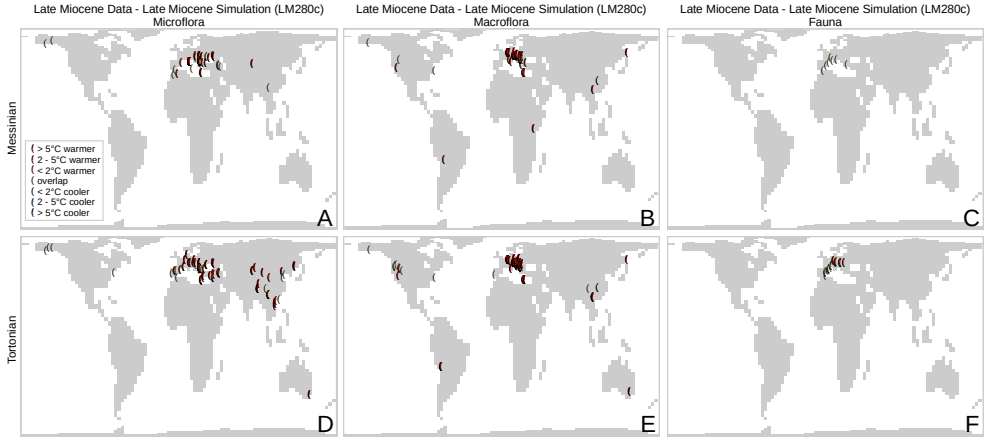

Fig. 8. Results from the model–data comparison for mean annual temperature, late Miocene data–LM280c.

importance of CO_2 uncertainties in determining late Miocene climate.

The numerical results from the model–data comparisons are given in Tables 2 and 3, and shown in Figs. 7–16.

5.1 Mean Annual Temperature

5.1.1 Late Miocene data compared to modern potential natural climate estimates

The differences in MAT we find between the late Miocene palaeodata and our modern climate estimates are shown in Fig. 7. The comparison shows that where we are confident that the MATs suggested by the palaeodata are different from our modern climate MAT estimates, they are significantly warmer; no datapoint is suggesting cooler temperatures in the late Miocene. There are 129 overlaps from a total of 429 datapoints (see Table 2). There is a clear difference in the microfaunal MAT reconstructions between the Tortonian and the Messinian (Fig. 7f compared to Fig. 7c). These results suggest that the Mediterranean Basin was much warmer in the Tortonian than today, but by the Messinian we are unable to confidently say that the MAT was any different than today. The same signal is perhaps apparent in the macroflora data in southwestern Europe and in South America (Fig. 7e compared to Fig. 7b) and in the microflora data in southwestern Europe (Fig. 7d compared to Fig. 7a).

5.1.2 Late Miocene data compared to the late Miocene simulations

Figure 8 and Table 2 show how well our LM280c simulation compares to the late Miocene MAT data reconstructions. Figure 8 clearly demonstrates that we are unable to generate the warm MATs suggested by the data for either the Messinian or the Tortonian by just changing the palaeogeography alone, and this finding is robust to the choice of proxy with microflora, macroflora and microfaunal proxies indicating the same results (Table 2, 117 overlaps from 429 datapoints).

Table 2. Results from the model–data comparison for modern and late Miocene palaeogeography.

Variable	Epoch	CTRLc-LMdata datapoints in agreement	LM280c-LMdata datapoints in agreement	Total number of LMdata datapoints	Number of LM280c improvements over CTRLc All data (overlaps)	Number of LM280c deteriorations over CTRLc All data (overlaps)	Net LM280c improvement over CTRLc All data (overlaps)	Percentage improvement LM280c over CTRLc All data (overlaps)
MAT (Macroflora)	Messinian	13	8	55	20(2)	27(7)	−7(−5)	−13(−9)
MAT (Microflora)		52	41	159	88(33)	62(44)	26(−11)	16(−7)
MAT (Fauna)		6	7	7	0(1)	0(0)	0(1)	0(14)
MAT (Macroflora)	Tortonian	17	18	90	43(8)	36(7)	7(1)	8(1)
MAT (Microflora)		28	29	98	53(14)	29(13)	24(1)	24(1)
MAT (Fauna)		13	14	20	6(1)	1(0)	5(1)	25(5)
MAT (All)	**late Miocene**	**129**	**117**	**429**	**210(59)**	**155(71)**	**55(−12)**	**13(−3)**
MAP (Macroflora)	Messinian	47	50	51	4(4)	1(1)	3(3)	6(6)
MAP (Microflora)		102	146	154	50(46)	3(2)	47(44)	31(29)
MAP (Fauna)		129	135	143	14(7)	1(1)	13(6)	9(4)
MAP (Macroflora)	Tortonian	69	75	79	9(7)	2(1)	7(6)	9(8)
MAP (Microflora)		73	76	94	19(8)	6(5)	13(3)	14(3)
MAP (Fauna)		432	482	531	96(57)	10(7)	86(50)	16(9)
MAP (All)	**late Miocene**	**852**	**964**	**1052**	**192(129)**	**23(17)**	**169(112)**	**16(11)**
CMT (Macroflora)	Messinian	31	38	48	16(11)	5(4)	11(7)	23(15)
CMT (Microflora)		106	135	142	36(34)	5(5)	31(29)	22(20)
CMT (Macroflora)	Tortonian	53	57	74	18(13)	12(9)	6(4)	8(5)
CMT (Microflora)		45	59	68	23(18)	4(4)	19(14)	28(21)
CMT (All)	**late Miocene**	**235**	**289**	**332**	**93(76)**	**26(22)**	**67(54)**	**20(16)**
WMT (Macroflora)	Messinian	0	2	48	27(2)	21(0)	6(2)	13(4)
WMT (Microflora)		5	9	143	15(5)	124(1)	−109(4)	−76(3)
WMT (Macroflora)	Tortonian	2	6	72	47(4)	23(0)	24(4)	33(6)
WMT (Microflora)		23	31	69	31(8)	15(0)	16(8)	23(12)
WMT (All)	**late Miocene**	**30**	**48**	**332**	**120(19)**	**183(1)**	**−63(18)**	**−19(5)**
Megabiome	Tortonian	124	123	314	N/A(19)	N/A(20)	N/A(−1)	N/A(0)
Megabiome	**late Miocene**	**229**	**222**	**556**	**N/A(34)**	**N/A(41)**	**N/A(−7)**	**N/A(−1)**

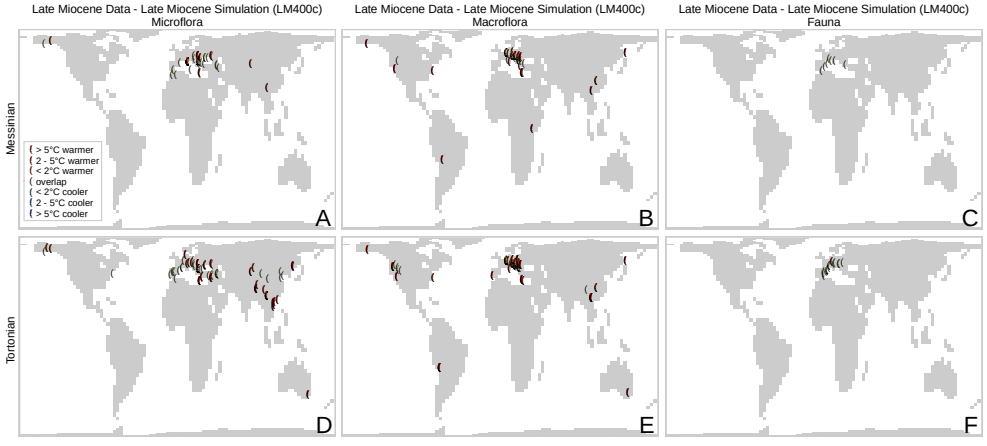

Fig. 9. Results from the model–data comparison for mean annual temperature, late Miocene data–LM400c.

The LM400c simulation, which includes both a palaeogeographic change and a CO_2 change, provides a better match to the data overall (Fig. 9, Table 3, 271 overlaps from 429 datapoints), with overlap between the modelled MATs and all but one of the Tortonian faunal-based MAT reconstructions (Fig. 9f). It is also noticeable that the model–data comparison for the Messinian aged microflora datapoints results in many more overlaps than the similar comparison with Tortonian aged data (Fig. 9a compared to Fig. 9d). Despite these improvements in the model–data comparison, there are still many datapoints which indicate warmer MATs than the LM400c simulation is able to model.

In summary, Fig. 10a and b show that there are regions where the palaeogeographic changes have resulted in improvements in the model–data comparison (e.g. northwestern America, midwestern Europe) and regions where the changes have resulted in deteriorations (e.g. northern and southern extents of the European data, southeast Asia, Australia). Table 2

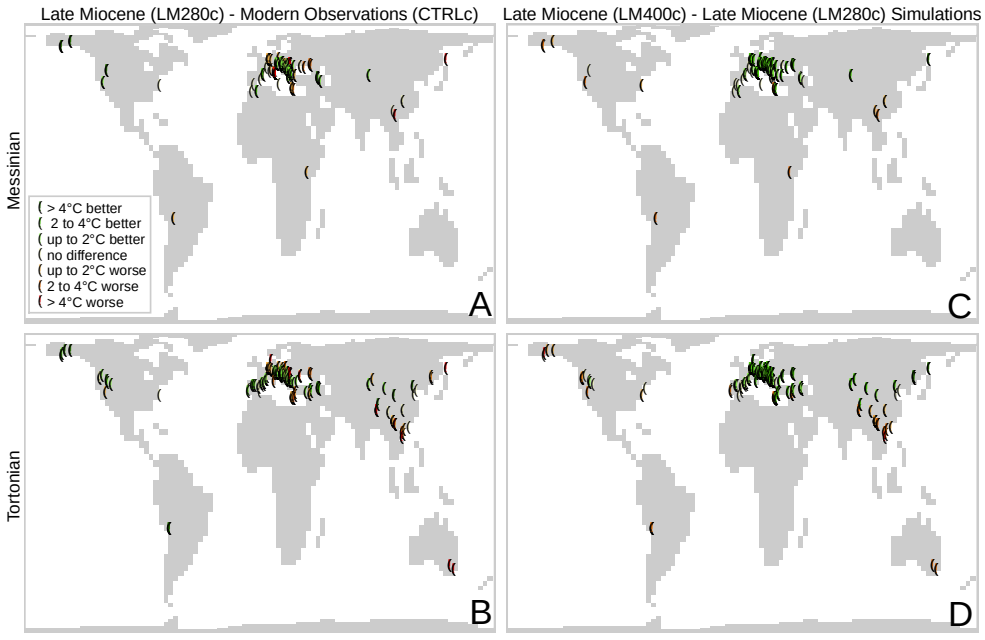

Fig. 10. Improvements in the model–data comparison for mean annual temperature. The lefthand column **(A, B)** shows the improvement that the late Miocene palaeogeography makes to the model–data comparison. The righthand column **(C, D)** shows the improvement that higher CO_2 makes to the model–data comparison. Green circles indicate an improvement; red circles indicate a deterioration. The datapoints showing "no difference" are plotted underneath the other datapoints in order to highlight the differences.

Table 3. Results from the model–data comparison for high and low CO_2 concentration assumptions.

Variable	Epoch	LM280c-LMdata datapoints in agreement	LM400c-LMdata datapoints in agreement	Total number of LMdata datapoints	Number of LM400c improvements over LM280c All data (overlaps)	Number of LM400c deteriorations over LM280c All data (overlaps)	Net LM400c improvement over LM280c All data (overlaps)	Percentage improvement LM400c over LM280c All data (overlaps)
MAT (Macroflora)	Messinian	8	34	55	39(29)	9(3)	30(26)	55(47)
MAT (Microflora)		41	101	159	116(0)	3(2)	113(−2)	71(−1)
MAT (Fauna)		7	7	7	0(0)	0(0)	0(0)	0(0)
MAT (Macroflora)	Tortonian	18	51	90	63(43)	18(10)	45(33)	50(37)
MAT (Microflora)		29	59	98	56(41)	25(11)	31(30)	32(31)
MAT (Fauna)		14	19	20	6(5)	0(0)	6(5)	30(25)
MAT (All)	**late Miocene**	**117**	**271**	**429**	**280(180)**	**55(26)**	**225(154)**	**52(36)**
MAP (Macroflora)	Messinian	50	49	51	1(0)	1(1)	0(−1)	0(−2)
MAP (Microflora)		146	147	154	5(1)	2(0)	3(1)	2(1)
MAP (Fauna)		135	135	143	7(0)	1(0)	6(0)	4(0)
MAP (Macroflora)	Tortonian	75	76	79	4(2)	1(1)	3(1)	4(1)
MAP (Microflora)		76	75	94	15(1)	4(2)	11(−1)	12(−1)
MAP (Fauna)		482	483	531	24(5)	29(4)	−5(1)	−1(0)
MAP (All)	**late Miocene**	**964**	**965**	**1052**	**56(9)**	**38(8)**	**18(1)**	**2(0)**
CMT (Macroflora)	Messinian	38	42	48	10(7)	3(3)	7(4)	15(8)
CMT (Microflora)		135	141	142	7(7)	1(1)	6(6)	4(4)
CMT (Macroflora)	Tortonian	57	65	74	17(11)	3(3)	14(8)	19(11)
CMT (Microflora)		59	64	68	7(7)	4(2)	3(5)	4(7)
CMT (All)	**late Miocene**	**289**	**312**	**332**	**41(32)**	**11(9)**	**30(23)**	**9(7)**
WMT (Macroflora)	Messinian	2	13	48	46(11)	0(0)	46(11)	96(23)
WMT (Microflora)		9	14	143	134(5)	0(0)	134(5)	94(3)
WMT (Macroflora)	Tortonian	6	23	72	66(17)	0(0)	66(17)	92(24)
WMT (Microflora)		31	43	69	38(12)	0(0)	38(12)	55(17)
WMT (All)	**late Miocene**	**48**	**93**	**332**	**284(45)**	**0(0)**	**284(45)**	**86(14)**
Megabiome	Messinian	99	119	242	N/A(39)	N/A(19)	N/A(20)	N/A(8)
Megabiome	Tortonian	123	158	314	N/A(58)	N/A(23)	N/A(35)	N/A(11)
Megabiome	**late Miocene**	**222**	**277**	**556**	**N/A(97)**	**N/A(42)**	**N/A(55)**	**N/A(10)**

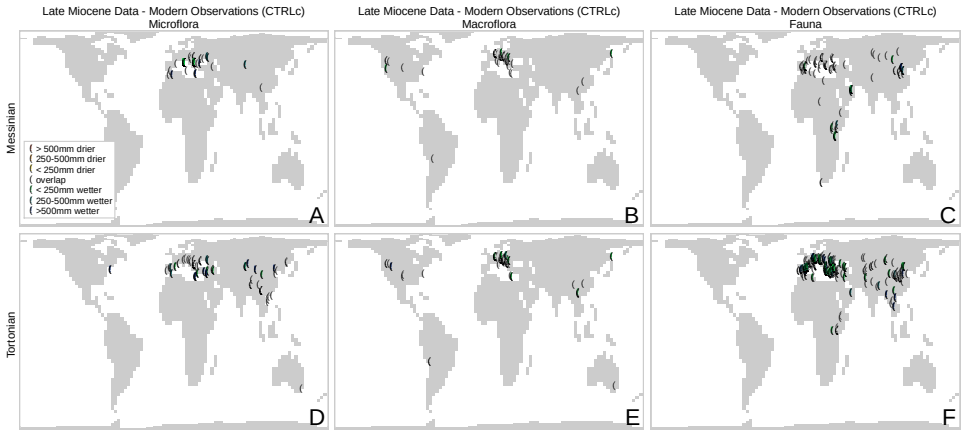

Fig. 11. Results from the model–data comparison for mean annual precipitation, late Miocene data–modern potential natural climate estimates.

details that the palaeogeographic changes result in a simulation that overlaps less with the MAT data than the modern potential natural climate estimates overlap (a reduction of 12 overlaps, or 3 %), but that overall the modelled MATs are closer to the data reconstructions (13 % better) due to improvements in the distance to overlap, mostly seen in the model–data comparison of Tortonian-aged datapoints.

Fig. 10c and d demonstrate the impact that CO_2 uncertainty has on the model–data comparison. They clearly show that the MATs of LM400c are an improvement in their match to the data reconstructions compared to the MATs of LM280c (Table 3, 225 datapoints are closer to model–data overlap in the LM400c than the LM280c – an improvement of 52 % overall, and a 36 % improvement in the number of overlaps). However, the data are very spatially biased towards Europe, and Fig. 10c and d also show that outside of Europe and mideastern Asia, the model–data comparison actually deteriorates as a result of the increased CO_2 concentration.

These results suggest that changing the palaeogeography to that appropriate for the late Miocene and increasing the CO_2 concentration from that of the modern potential natural climate together results in a model simulation that is able to reproduce much of the warm European MATs (Fig. 9), but that it is unable to entirely reproduce the warm MATs indicated by the late Miocene data elsewhere.

5.2 Mean Annual Precipitation

5.2.1 Late Miocene data compared to modern potential natural climate estimates

The comparison between the late Miocene data and the modern climate estimates for precipitation are shown in Fig. 11. The MAP data reconstructions suggest that where we are confident that the climate of the late Miocene is different from a potential natural modern one, the MAPs are wetter; none of the datapoints suggest drier MAPs in the late Miocene. There are a large number of overlaps between the late Miocene MAP data and the modern MAP estimates (Table 2, 852 overlaps from a total of 1052 datapoints). The faunal Tortonian data reconstruct a much wetter climate in Europe (Fig. 11f), whereas the Messinian data reconstructions in this region are largely similar to today (Fig. 11c). A similar pattern is perhaps seen in the microflora and macroflora MAP reconstructions in this area (Fig. 11d compared to Fig. 11a; Fig. 11e compared to Fig. 11b).

5.2.2 Late Miocene data compared to the late Miocene simulations

The LM280c simulation compares well to the reconstructed MAPs (Fig. 12; Table 2, 964 overlaps from 1052 datapoints), and of the macroflora reconstructions, just 5 datapoints do not overlap (Fig. 12b and e; Table 2). The 88 datapoints which do not overlap with the modelled MAPs are wetter than the model predicts.

There is a significant improvement in the model–data comparison for MAPs when compared with the modern climate comparison (Fig. 12 compared to Fig. 11; Table 2, 192 improvements versus just 23 deteriorations), suggesting that changing the palaeogeography alone takes the modelled MAPs closer to the reconstructed MAPs.

Although the LM400 simulation predicts generally an increase in the MAP as compared to the LM280 simulation (Fig. 5d–f), both the simulations result in MAP predictions that are within the uncertainty of the late Miocene MAP reconstructions, and therefore little change is seen in the model–data comparison for this variable between the two simulations (Fig. 13 compared to Fig. 12; Table 3, 964 overlaps for LM280c compared with 965 for LM400c). This suggests that the palaeogeographic changes we have made are the driving force behind the modelled precipitation changes observed, and that the CO_2 concentration plays only a minor

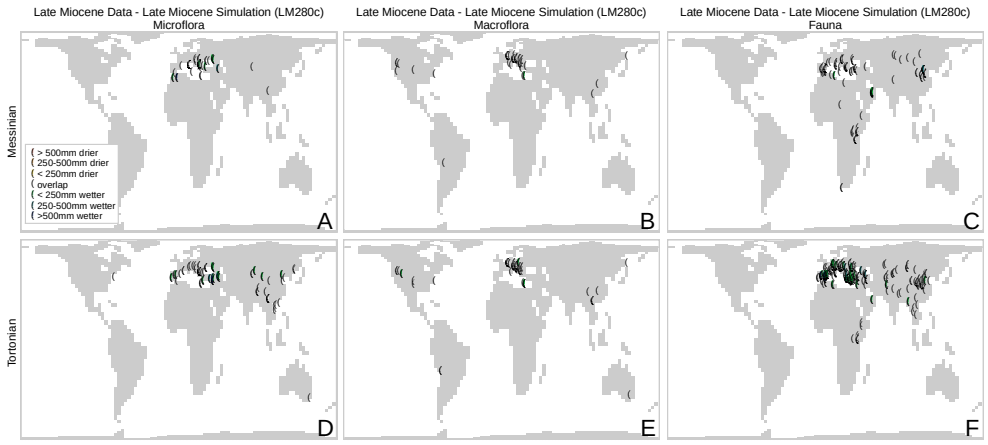

Fig. 12. Results from the model–data comparison for mean annual precipitation, late Miocene data–LM280c.

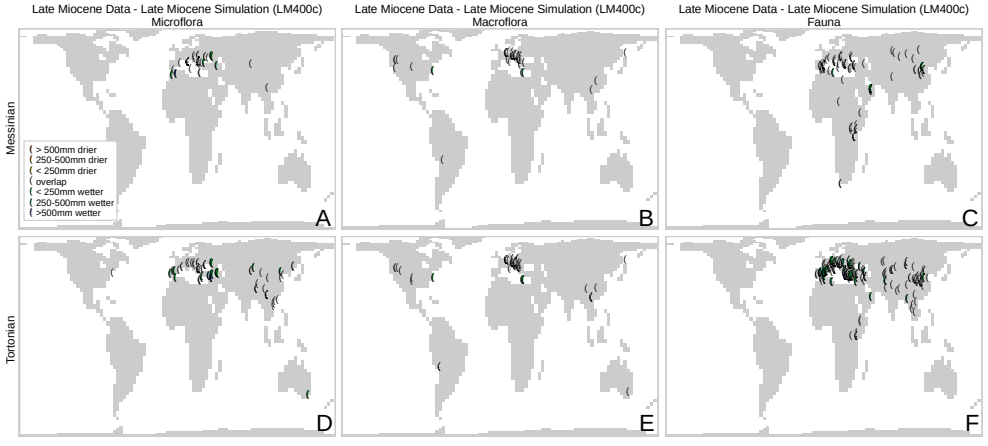

Fig. 13. Results from the model–data comparison for mean annual precipitation, late Miocene data–LM400c.

role. However, Fig. 14 demonstrates that many of the datapoints overlap both the LM280c modelled MAPs and those of our modern potential natural climate. In fact, Fig. 14c and d demonstrates that many of the datapoints in western Europe are further from overlap with the LM400c modelled MAPs than they are with the LM280c modelled MAPs, indicating that higher CO_2 may actually worsen model–data comparison in this region.

5.3 Mean Cold Month Temperature

5.3.1 Late Miocene data compared to modern potential natural climate estimates

The comparison between the late Miocene data and the modern climate estimates for the CMT are shown in Supplement Fig. S1. The CMT data reconstructions suggest that where we are confident that the climate of the late Miocene is different from a potential natural modern one, the CMTs are wamer; none of the datapoints suggest cooler CMTs in the late Miocene. There are many overlaps between the late Miocene CMT data and the modern CMT estimates (Table 2, 235 overlaps from a total of 332 datapoints).

5.3.2 Late Miocene data compared to the late Miocene simulations

The LM280c simulation compares reasonably well to late Miocene CMT data (Supplement Fig. S2; Table 2, 289 overlaps from a total of 332 datapoints), and the LM400c simulation compares even better, especially to the microflora reconstructions (Supplement Fig. S3; Table 3, 312 overlaps from a total of 332 datapoints). The palaeogeographic changes made account for a 16 % improvement in the number of overlaps, and the CO_2 concentration changes account for an additional 7 % improvement as compared to the modern climate estimates (Supplement Fig. S4; Tables 2 and 3).

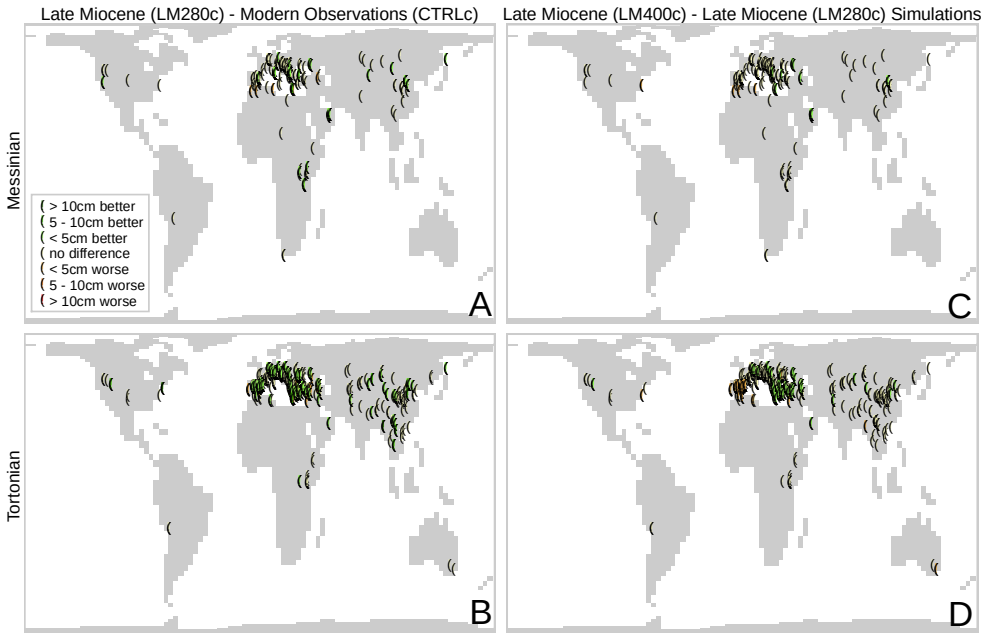

Fig. 14. Improvements in the model–data comparison for mean annual precipitation. The lefthand column **(A, B)** shows the improvement that the late Miocene palaeogeography makes to the model–data comparison. The righthand column **(C, D)** shows the improvement that higher CO_2 makes to the model–data comparison. Green circles indicate an improvement; red circles indicate a deterioration. The datapoints showing "no difference" are plotted underneath the other datapoints in order to highlight the differences.

5.4 Mean Warm Month Temperature

5.4.1 Late Miocene data compared to modern potential natural climate estimates

The comparison between the late Miocene data and the modern climate estimates for the WMT are shown in Supplement Fig. S5. With the exception of southeast Asia, the WMT data reconstructions suggest that the WMTs were significantly warmer in the late Miocene than in the potential natural modern climate. There are few overlaps between the late Miocene WMT data and the modern WMT estimates (Table 2, just 30 overlaps from a total of 332 datapoints).

5.4.2 Late Miocene data compared to the late Miocene simulations

The LM280c simulation fails to reproduce the warmer temperatures reconstructed by the WMT data for the late Miocene (Supplement Fig. S6; Table 2, 48 overlaps from a total of 332 datapoints), but the LM400c simulation compares better, particularly for the western Mediterranean (Supplement Fig. S7). The palaeogeographic changes made account for a 5 % improvement in the number of overlaps, and the CO_2 concentration changes made account for an additional 14 % improvement (Supplement Fig. S8; Tables 2 and 3).

5.5 Megabiomes

5.5.1 Late Miocene data compared to modern potential natural climate estimates

Figure 15a and d show the comparison between the megabiomes derived from the BIOME4 model driven by the modern control simulation CTRLc and the Messinian data, and Fig. 15g and j show the comparison between the megabiomes derived from the BIOME4 model driven by the modern control simulation CTRLc and the Tortonian data. There are some large vegetation shifts documented at the biome level (Pound et al., 2011, 2012), and when aggregated to megabiome level, the vegetation shifts between the late Miocene and today are still noticeable, but in fact there are only 229 overlaps from a total of 556 datapoints (Table 2). There are many regions where there are significant differences in the megabiomes predicted for the late Miocene and today, including northwest America and northeast Asia, Greenland and northern Europe, the Mediterranean Basin, central Asia, southern and southeastern Asia, South America, South Africa, and Australia/New Zealand.

5.5.2 Late Miocene data compared to the late Miocene simulations

Figure 15b and e show the comparison between the Messinian megabiomes and those predicted by the BIOME4

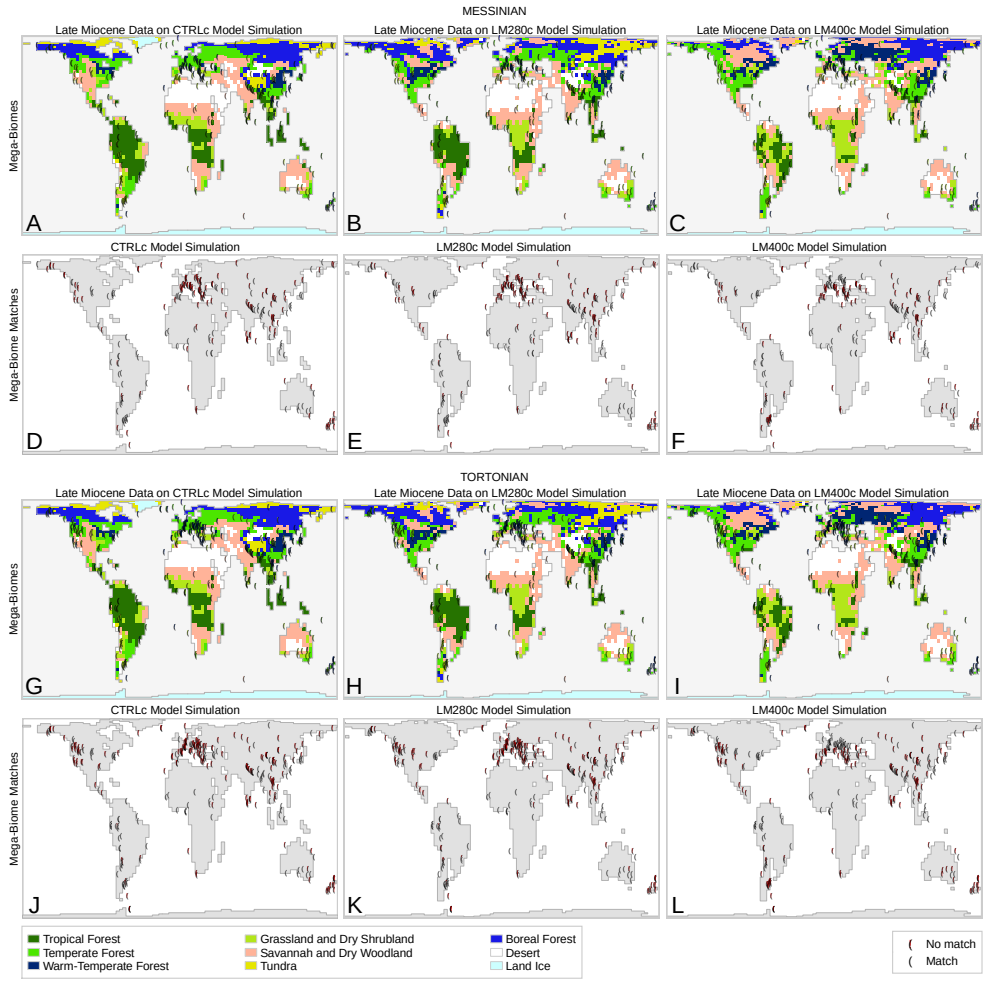

Fig. 15. Results from the model–data comparison for megabiomes: late Miocene data on CTRLc, LM280c, and LM400c

model driven by the LM280c simulation, and Fig. 15h and k show the comparison between the Tortonian megabiomes and those predicted by the BIOME4 model driven by the LM280c simulation. Little difference is seen between the comparison with the Messinian age data and the Tortonian age data. As discussed in Sect. 4.2.3, the BIOME4 model predicts quite a significant change in the vegetation of Central America; however, the megabiome data do not support this change (Fig. 15b compared to 15a, and 15h compared to 15j), suggesting that perhaps the response of the model to the open Panama gateway is too strong, or that our simulated Panama gateway is too wide. The LM280c simulates a change from the modern tropical forests of central Africa to grasslands and dry shrubland, but unfortunately there are no datapoints in this region in order to verify this change. The LM280c simulation also results in a shift from the modern boreal forest to tundra in northeastern Asia, but the datapoints in this region do not support this change (Fig. 15b and e, and 15h and k). Compared to the CTRLc simulation, the LM280c simulation does not improve the model–data comparison for most datapoints, and in fact, overall the comparison worsens very slightly (Fig. 16a and c; Table 2, 34 improvements versus 41 deteriorations, a worsening of 1 %).

Figure 15c and f show the comparison between the Messinian megabiomes and the LM400c simulation, and Fig. 15i and l show the comparison between the Tortonian megabiomes and the LM400c simulation. The megabiomes are in agreement for many of the datapoints of northwest America and north and east Asia that disagreed with the CTRLc simulation (Fig. 15f, and to a lesser extent Fig. 15l). There are 277 agreements between the megabiomes reconstructed by the data and the LM400c simulation, from 556 datapoints in total. The 279 datapoints that disagree with this simulation are located mainly in central, southern and southeastern Asia, and the land surrounding the Mediterranean Basin. When compared to the LM280c simulation, the model–data comparison worsens in South America in particular (Fig. 16b and d). Overall though, the LM400c

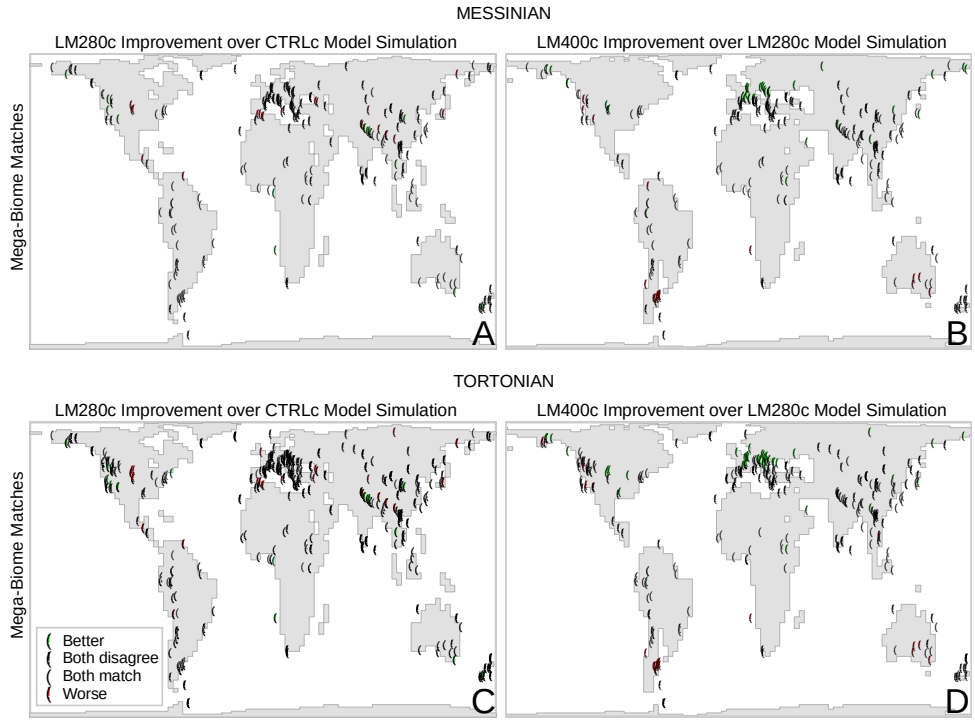

Fig. 16. Improvements in the model–data comparison for megabiomes. Panels **(A)** and **(C)** show the improvement that the late Miocene palaeogeography makes to the model–data comparison. Panel **(B)** and **(D)** show the improvement that higher CO_2 makes to the model–data comparison. Green circles indicate an improvement; red circles indicate a deterioration.

simulation offers a 10 % improvement over the LM280c (Table 3).

5.6 Discussion

We ask the question to what extent the different palaeogeography of the late Miocene can explain the differences in the climate documented in the palaeorecord, and how important is the uncertainty in the atmospheric CO_2 concentration?

The results from the model–data comparison for the MAT are difficult to interpret. Table 2 details that a large number of improvements and a large number of deteriorations exist as a result of the palaeogeographic changes made. The Messinian data generally suggests that the palaeogeographic changes are not able to improve the model–data comparison as compared to the modern potential climate estimates, but the Tortonian data generally suggests the opposite. However, overall there are more datapoints closer to overlap with the late Miocene simulation LM280c than the modern potential natural climate estimates, but the total number of overlaps reduces as a result of palaeogeographic change (Fig. 17). However, Fig. 17 demonstrates that the atmospheric CO_2 concentration is very important in determining the MATs of the late Miocene, with large improvements seen for both the Messinian and Tortonian model–data comparison as a result of increasing the assumed CO_2 concentration. Furthermore, the higher CO_2 assumption combined with the palaeogeographic changes made in the LM400c simulation offers a significant improvement in the model–data comparison when compared to the modern potential natural climate estimates with nearly twice as many overlaps with the datapoints (Table 3). This finding is consistent with similar model–data comparison work for the preceding middle Miocene (Krapp and Jungclaus, 2011), and is also consistent with the model–data comparison for the CMT and WMT (Fig. 18). In order to test the robustness of this result, an additional comparison is made with the CTRL simulation with 400 ppm atmospheric CO_2 (hereafter referred to as CTRL400c). Supplement Fig. S9 shows that the CTRL400c simulation has a comparable (and, in fact, slightly higher) number of overlaps with the late Miocene data to the LM400c simulation, and 172 more overlaps than the modern potential natural climate estimates, further supporting the importance of atmospheric CO_2 in determining the MATs.

Figure 17 shows that the different late Miocene palaeogeography is important in determining the different MAPs for both the Messinian and the Tortonian stages, because all of the proxy reconstructions considered show an improvement in the model–data comparison for the late Miocene simulation as compared to the modern potential climate estimates (Table 2). Figure 17, however, suggests that the uncertainty in the atmospheric CO_2 concentration is not important

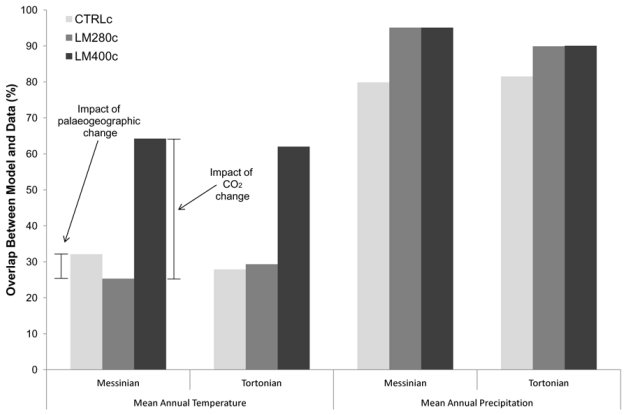

Fig. 17. Model–data comparison summary for MAT and MAP. Shown is the percentage of the total number of datapoints that overlap with the model results.

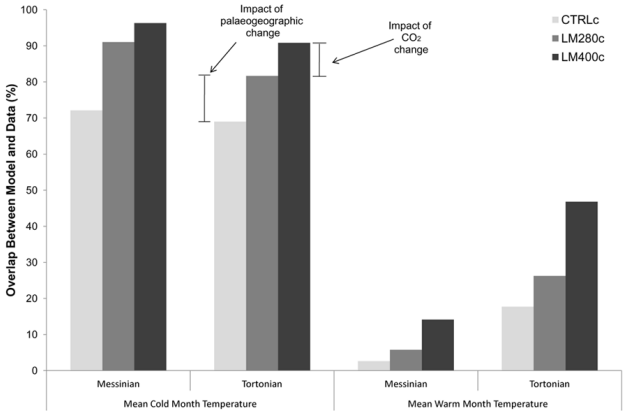

Fig. 18. Model–data comparison summary for CMT and WMT. Shown is the percentage of the total number of datapoints that overlap with the model results.

in determining the different MAPs documented for the late Miocene, as only very small differences are found between the results of LM400c and LM280c (Table 3). The locations where LM280c compares better to the MAP reconstructions than the modern potential climate estimates are spread across the spatial range of the dataset (North America, Europe, Asia, Africa), and therefore it is difficult, without the use of further sensitivity studies, to relate these improvements definitively to a particular palaeogeographic change. Although an open Panama gateway can be linked to reduced precipitation across most of Europe and Asia, it can also be linked to a pocket of increased precipitation centred over modern day Myanmar (see Fig. 9 of Lunt et al., 2008b), which is consistent with our LM280c simulation and is the locality for some of the improvements obtained in the MAP model–data comparison. We can, however, probably rule out both the retreat of the Paratethys Sea and the uplift of the Himalayas for the southern and eastern Asian improvements in the MAP model–data comparison, as these palaeogeographic changes have been shown to result in increased precipitation in India and China (e.g. Ramstein et al., 1997; Lunt et al., 2010; Zhang et al., 2007a, b). These changes could, however, be related to some of the improvements seen in western Asia (refer to Fig. 6 of Ramstein et al., 1997; and Fig. 2b and c of Fluteau et al., 1999) and in Europe (refer to Fig. 2b and c of Fluteau et al., 1999). The further improvements in the MAP model–data comparison across Asia could therefore be related to changes made to the Indonesian seaway, and the improvements across Europe related to the elevation changes made in Europe itself (e.g. Henrot et al., 2010) and also perhaps related to the additional late Miocene eurasian landmass. Further sensitivity studies are requried to test these hypotheses. The megabiome results show very little difference in the model–data comparison with the late Miocene simulation LM280c as compared to the model–data comparison with the control simulation CTRLc. However, there is an improvement in the megabiome model–data comparison for the higher CO_2 simulation as compared to the lower CO_2 simulation, again suggesting that atmospheric CO_2 concentration is an important consideration.

Our modelling results are in general agreement with those of other similar studies (Knorr et al., 2011; Micheels et al., 2011) in that palaeogeographic changes for the late Miocene causes regions of warming in the areas of orographic change, and regions of cooling, particularly in the North Atlantic. A recent study has found that vegetation changes are very important in determining the late Miocene climate, perhaps three times more important than the palaeogeographic changes (Knorr et al., 2011). They find reasonable agreement between their late Miocene model simulation with preindustrial atmospheric CO_2 concentrations and the palaeorecord when the vegetation used in the model is prescribed, thereby reconciling a warmer climate with low CO_2 concentrations. The benefit of a coupled GCM–vegetation model is that the simulated vegetation distribution will be in equilibrium with the modelled climate, but the disadvantage is that the simulated vegetation will not match the palaeodata if the climate is incorrectly modelled. The relative impacts of vegetation changes versus CO_2 changes from this model, and the implications for the findings presented here, will be explored in future work.

The megabiome model–data comparison results for LM400c show that some of the documented extreme changes in vegetation are captured by the BIOME4 model when forced by this simulation. BIOME4/LM400c predicts temperate forests in what is now the circumboreal region, consistent with Denk et al. (2005) and Worobiec and Lesiak (1998), and grasslands in the Arabian peninsula, consistent with Kingston and Hill (1999). However, despite the improvements that we find in the model–data comparison for changing palaeogeography and for changing the CO_2 assumption, significant model–data inconsistencies remain.

6 Summary and conclusions

6.1 Summary

We have simulated two potential late Miocene climates using the fully coupled atmosphere–ocean–vegetation GCM model HadCM3L-TRIFFID. Both simulations assume a palaeogeography appropriate for the late Miocene, but one has preindustrial levels of CO_2 at 280 ppm and the other a slightly higher CO_2 concentration at 400 ppm. We compare the 280 ppm late Miocene simulation against a modern control simulation with the same preindustrial level of CO_2 in order to investigate the potential role of palaeogeography in determining the simulated late Miocene climate. We also compare the two late Miocene climate simulations to investigate the role of CO_2 in determining the simulated climates.

The global anomaly between the two 280 ppm climatologies is close to zero for both MAT and MAP, but there are significant regional differences. Our late Miocene palaeogeographic changes have been found to alter the climate; for example, there is a large area of cooler drier air that spreads across the North Atlantic Ocean into Eurasia for the late Miocene, the lapse rate effect on temperature results in regional warming in areas of topographic lowering for the late Miocene, and significant reductions in late Miocene monsoonal precipitation are modelled.

A database containing 1030 terrestrial proxy records for the late Miocene has been compiled from the literature. From these data we infer a substantially warmer and wetter late Miocene climate as compared to a potential modern natural climate. We have made quantitative comparisons of these data and the biome data (Pound et al., 2011, 2012) to both our late Miocene simulations and our potential modern natural climate estimates in order to investigate the extent to which palaeogeographic changes alone can explain late Miocene climate and to examine the importance of the uncertainty in the CO_2 palaeorecord.

We have used proxy data from a variety of different reconstruction methods, and overlap between different methods of climate reconstruction used on the same proxy data indicate reliability, but ideally overlap between entirely independent proxies is desirable. We therefore also recommend, where possible, the expansion and better temporal constraint of the multiproxy palaeorecord for the late Miocene, in particular for the regions where the model–data inconsistencies are largest, and a more robust and consistent assessment of uncertainties in all proxy records. We have tried to account as much as possible for uncertainties in the proxy reconstructions, so we have some confidence that the reconstructed signals are robust. However, we cannot rule out significant errors in our palaeogeographic reconstruction and/or the model itself. We will conduct future modelling with the same coupled atmosphere–ocean–vegetation GCM in order to establish sensitivity to our choice of palaeogeographic configuration on the simulated climate, and also the relative roles of CO_2 concentration versus vegetation distribution.

6.2 Conclusions

Despite the uncertainties in proxy data reconstructions and the limited distribution and spatial/temporal bias of the palaeorecord, we do find significant evidence to suggest that the palaeogeography can have an important role in determining aspects of the late Miocene climate, particularly for the MAP for both the Messinian and the Tortonian. However, the uncertainty in the palaeo-CO_2 record is also important because the sensitivity model simulation, CTRL400c, suggests that both the palaeogeography and the atmospheric CO_2 contribute to determining the MAP, but that they do not add linearly. The megabiome model–data comparisons show some improvements as a result of the palaeogeographic alterations on the west coast of North America, in Australasia, southeast Europe and eastern Asia. We find significantly better model–data consistency for the higher CO_2 late Miocene simulation than for the lower CO_2 simulation for the both Messinian and Tortonian MATs but only modest differences for the MAP of both stages. We therefore conclude that the MAP differences can be driven by either the palaeogeographic changes made, or by the atmospheric CO_2 changes made. However, given that the temperature differences are very strongly influenced by the CO_2 concentration, it is perhaps likely that late Miocene atmospheric CO_2 concentrations were generally nearer the high end of the range of reconstructions, and that palaeogeography plays a much more localised role in determining late Miocene temperatures.

Appendix A

Uncertainty in late Miocene proxy reconstructions

As a multi-proxy dataset is used, there is considerable variability in the age constraint due to uncertainty in the dating, and many datapoints are only consigned to the Messinian or the Tortonian. Ages used were from Pangaea (http://www.pangaea.de) or the original paper where available, otherwise we used ages for mammal zones or geoglogical stages as given in the Paleobiology Database (http://paleodb.org) or in Bernor et al. (1993). Age data for large mammal data derived from the NOW database follows the NOW database dating scheme, based on Steininger (1999). The data is considered in 2 timeslabs, the Messinian (5.3–7.25 Ma) and the Tortonian (7.25–11.6 Ma), and any datapoints that overlap both stages in their age uncertainty were duplicated, one datapoint placed in each stage. Likewise, any datapoints with age uncertainty ranges spanning the Messinian into the Pliocene were placed in our Messinian database, and any datapoints with age uncertainty ranges spanning the Tortonian into the middle Miocene were placed in our Tortonian database. We

note that the proxy data used is likely to have been generated under a range of different orbital configurations and other climatic cycles such as El Niño (Galeotti et al., 2010), and individual datapoints could therefore represent extremes in these cycles; however, this is unlikely to have biased the entire dataset. There is some evidence that vegetation proxies give slightly higher estimates than palaeozoological climate recontructions (see Eronen et al., 2012). In the dry parts of climate cycles, the preservation potential of plant remains and organic matter in general is low (for discussion see Bruch et al., 2011; Eronen et al., 2012), and even palynomorphs consisting of comparatively chemically resistant sporopollenin may not outlast highly oxidizing conditions. Hence, the fossil plant record might represent the wetter part of a climate cycle. On the other hand, deposits like coarser clastic successions favor preservation of fossilized mammals in arid habitats over closed forest.

For a comparison study between fossil data and GCM simulations where a palaeontological assemblage has been used to reconstruct climatic conditions, such as the MAT or MAP, two main uncertainties exist in the reconstructions: taphonomical (the death, decay, deposition and preservation of fossils) and the uncertainties associated with the data reconstruction techniques. Below, we discuss comparisons between different techniques. For full details on each technique and detailed taphonomical biases in each case, the reader is referred to the original publications (Taphonomy: Western and Behrensmeyer, 2009; Martin, 1999; Behrensmeyer et al., 2000. Data reconstruction techniques: Mosbrugger and Utescher, 1997; Fauquette et al., 2006; Wolfe, 1993; Spicer, 2007; Spicer et al., 2009; Eronen et al., 2010; Jacobs and Deino, 1996; Montuire et al., 2006; Böhme et al., 2008; van Dam, 2006).

The majority of palaeobotanical climate reconstructions used in this study come from two techniques, the co-existence approach and CLAMP. The co-existence approach uses a Nearest Living Relative (NLR) philosophy: the climate tolerance of a fossil taxons closest extant relative is likely to be comparable to that of the fossil (Mosbrugger and Utescher, 1997). From this idea an assemblage of fossils can be compared to find the overlapping climate space that all taxa could have survived in, based on the climate tolerances of each fossils nearest living relative (Mosbrugger and Utescher, 1997). CLAMP is the latest iteration of the plant physiognomy philosophy that has been known for almost a century: plants vary their structure with climate, in a non-random way (Bailey and Sinnott, 1915; Holdridge, 1947). CLAMP uses leaf morphology to reconstruct quantitative climate information using "training sets" from undisturbed modern day floras (Spicer et al., 2009; Yang et al., 2011). It is known that the leaf physiognomic techniques (e.g. CLAMP) produce lower MAT estimates than the co-existence approach (Mosbrugger and Utescher, 1997; Uhl et al., 2003, 2006, 2007). Reasons for this are still unknown (but see Uhl, 2007, for discussion). On the other hand, the co-existence approach produces estimates that are comparable to each other, which limits the bias in our dataset. For more extensive comparison between different palaeobotanical proxy methods, see Thiel et al. (2012).

The palaeozoological climate reconstructions come from very different techniques. For small mammals the basis is taxonomy: species richness is related to climate parameters for small mammals (Montuire et al., 2006; van Dam, 2006; Böhme et al., 2008). For large mammals the reconstruction technique is based on traits that are not determined by taxonomy, but by morphology: the tooth morphology of herbivores is related to the vegetation abrasiveness and other wearing agents. These are mainly controlled by water-stress and climate, and therefore these characteristics can be used to derive palaeoprecipitation estimates from large herbivores (Eronen et al., 2010).

As the climate reconstruction techniques are derived from different sources, there are both age and location uncertainties to consider in making a comparison between the estimates of each technique. It is fairly rare to have cases where multiple evidence sources are available. There is some indication that at the locality level these techniques produce overall agreement (see discussion in van Dam, 2006, p. 200). The initial results from a larger comparison between large mammal estimates and vegetation proxies using pooled regional data also show overall agreement (Eronen et al., 2012, but see discussion above).

Appendix B

Model details

B1 HadCM3L GCM

B1.1 Description

The model contains many parameterizations of atmospheric and oceanic processes, including atmospheric convection (Gregory and Rowntree, 1990), boundary layer mixing (Smith, 1993), ocean layer mixing (Gent and McWilliams, 1990), and radiation (Edwards and Slingo, 1996). HadCM3L has been used in studies of the future (e.g. Cox et al., 2000) and the past (e.g. Lunt et al., 2007, 2010). As HadCM3L has a reduced ocean resolution, model performance is degraded compared to HadCM3. For example, the ocean resolution of HadCM3L is such that the Denmark Straits are unresolved, and therefore the two terrestrial grid points representing Iceland are removed to prevent an unacceptable build up of sea ice in the Nordic Sea (Jones, 2003). The version of HadCM3L used here does not therefore require the inclusion of flux corrections to maintain a stable overturning circulation for the modern ocean (Jones, 2003).

The model land surface processes are simulated using the MOSES-2.1 (Met Office Surface Exchange Scheme) land

surface scheme (Essery and Clark, 2003). There are nine surface types, five of which correspond to plant functional types (PFTs) – broadleaf tree, needleleaf tree, C_3 grass, C_4 grass and shrub – and the remainder representing bare soil, water bodies, ice and urban surfaces.

B1.2 Uncertainties

No GCM is able to reproduce exactly the modern climate, and a discussion of the biases in the HadCM3 version of our GCM is given in Gordon et al. (2000). The HadCM3L version of the model suffers from temperature biases, particularly too-cool ocean temperatures at high latitudes. Temperatures over the land surface are generally within the 1–2 °C of the uncertainty of the CRU-TS 3.0 modern instrumental data (Mitchell and Jones, 2005), but there is still a marked cold bias at high northern latitudes of up to 10 °C above 70° N, and the regions of highest orography (Himalayas and Andes) are too warm by > 3 °C. Similar biases exist for precipitation, with the MAP being underestimated by up to a third in parts of northern South America and southern India, and overestimated by the same amount in some tropical regions of South America, Africa and Australia.

B2 TRIFFID vegetation model

B2.1 Description

TRIFFID calculates areal coverage, leaf area index and canopy height for the five PFTs, which each respond differently to climate and CO_2 forcing, and all can co-exist within the same gridbox.

Two modes of coupling between the TRIFFID and the GCM are used: an equilibrium mode used during model spin-up, in which the fluxes between the land and the atmosphere are calculated by the GCM and averaged over ~ 5 yr, and a dynamic mode, used for the last 100 yr of the simulations, in which the fluxes are averaged over 10 days to include interannual variability. The averaged fluxes are then passed to TRIFFID which calculates the growth and expansion of the existing vegetation, and updates the land surface parameters based on the new vegetation distribution and structure.

B2.2 Uncertainties

TRIFFID is based on physiological constraints that influence vegetation distributions, and is therefore attempting to model the potential natural vegetation for a given climatology. Estimates of anthropogenic land surfaces (urban and agricultural) amount to some 16 % of the total land surface area (CIESIN, 2004; Matthews, 1983; Ramankutty and Foley, 1999; Schneider et al., 2009), and therefore discrepancies will exist in those areas between reference maps of reconstructed natural vegetation (the vegetation that might exist if human influence were to cease, based on extrapolation of remnants of natural vegetation) and model-produced maps of potential natural vegetation (the vegetation that might exist if human influence had never existed); these may be significant in areas of deforestation (Prentice et al., 1992).

The TRIFFID model has been compared to IGBP-DIS land cover dataset, which represents the modern distribution of vegetation as derived from satellite image interpretation (Loveland and Belward, 1997; Betts et al., 2004). This suggests that the shrub PFT is overestimated at high latitudes, that the broadleaf tree PFT is overestimated in equatorial regions, and that grasses tend to be globally slightly underestimated. The discrepancies between the satellite imagery and the TRIFFID model are suggested to be a combination of orographic representation leading to underestimation of precipitation, differences between the anthropogenic masks used in their version of the model and that found on the satellite imagery, and the inadequate treatment of natural disturbance mechanisms such as fire (Betts et al., 2004). The version of the model used here aims to reproduce the vegetation of a modern potential natural climate, and therefore evaluation of the predicted PFTs is difficult. It is also hard to identify when the modern predicted PFTs are likely wrong (e.g. needleleaf forests in southeast Asia and extensive broadleaf forests in Australia), whether those inadequacies are due to the climate model or the vegetation model, and it is likely that due to the interactive coupling between TRIFFID and HadCM3L, the existing GCM biases will be amplified in the vegetation predictions.

B3 BIOME4 vegetation model uncertainties

As with the TRIFFID model, the BIOME4 model is also based on physiological constraints that influence vegetation distributions, and therefore attempts to model the potential natural vegetation for a given climatology. The BIOME4 model has been shown to produce a fair comparison to the vegetation data of Olson et al. (1983), with most of the areas of discrepancy being attributed to differences between potential natural vegetation and actual modern vegetation as a result of human influence. Other suggested sources of error include incorrect climatological forcing due to the difficulty in representing orographic extremes, and missing parameterisations in the model, particularly related to seasonality (Prentice et al., 1992).

Appendix C

Model boundary conditions: modern configuration

For the modern control (CTRL) simulation, we use the standard UK Meteorological Office configurations for modern continental positions and both terrestrial and ice sheet elevations as defined in the ETOPO5 dataset (NOAA, 1988). Land ice grid boxes and soil type distributions used in CTRL are based on the identification of Wilson and Henderson-Sellers

(1985). The two land grid boxes that represent Iceland are converted to ocean grid boxes as discussed in Sect. 2.3.4.

We also use modern ETOPO5 bathymetry (NOAA, 1988). The two new ocean grid boxes replacing Iceland are assigned the average depth of the surrounding ocean grid boxes. We note that the land–sea mask generation algorithms that map the high resolution data onto the HadCM3L grid also result in the non-representation of many other small islands.

For the purpose of this study we wish to model a potential natural modern climate, and therefore assume a preindustrial atmospheric CO_2 concentration in the range 275–284 ppm (Etheridge et al., 1996) and use a value of 280 ppm in CTRL, consistent with the Climate Model Intercomparison Project standard (Meehl et al., 2007). Other greenhouse gases are also set to preindustrial levels of atmospheric gases (CH_4 = 760 ppb, N_2O = 270 ppb, CFCs = 0 ppt).

Appendix D

Late Miocene configuration

D1 Orography

The orography for the late Miocene has been reconstructed by Markwick (2007) using a methodology of establishing relationships between modern elevations and their tectonophysiographic settings and applying those same relationships to the geological record (a full description of the technique is described in Markwick, 2007, and Markwick and Valdes, 2004). The methodology results in significant reductions in the Miocene elevations of most of the world's highest regions compared to modern. We now describe those reductions in relation to the palaeoelevation estimates of other authors; however, given the uncertainties associated with reconstructing past mountain elevation (e.g. Ehlers and Poulsen, 2009), any inconsistencies with that of Markwick (2007) would require further sensitivity experiments.

The Tibetan Plateau in the late Miocene simulations is an average 30 % lower than in CTRL. The timing of Tibetan uplift is debated, with many studies indicating an elevation during the late Miocene similar to today (e.g. Currie et al., 2005; DeCelles et al., 2007; Spicer et al., 2003; Garzione et al., 2000; Rowley et al., 2001; Rowley and Currie, 2006). There is evidence that the uplift did not occur in a spatially uniform pattern (England and Searle, 1986; Clark et al., 2005; Rowley and Garzione, 2007), but a recent study has shown that modelled SSTs in the Indian and Pacific Oceans were very similar for three simulations assuming different uplift histories (Lunt et al., 2010).

The Andes are 45 % lower in the late Miocene simulations than the CTRL. This is consistent with palaeobotanical and geomorphological data which suggests that the elevation of the Andes was no more than half of the modern elevation at $\sim$ 11–10 Ma (Gregory-Wodzicki, 2000).

The Alps are on average 30 % lower in the late Miocene simulations than the CTRL. Palaeoaltitude estimates for the Eastern Alps are between 500 and 2000 m (Jimenez-Moreno et al., 2008; Kuhlemann, 2007). These estimates are consistent with the Markwick (2007) reconstruction.

The Western Cordillera of North America is on average 25 % higher in the late Miocene simulations than in the CTRL. The evolution of topographic changes in the Western Cordillera are debated. There is evidence for high elevation in the Western Cordillera of North America since the Eocene (Sjostrom et al., 2006) or even the Cretaceous (Chase et al., 1998), with the elevation in Nevada during the Middle Miocene being some 1–1.5 km higher than it is today. The dating of the collapse to present day elevation in Nevada is put at $\sim$ 13 Ma by Wolfe et al. (1997), but the palaeoelevation reconstruction from Markwick (2007) differs in that Nevada is $\sim$ 9 % lower in LM than CTRL. Orographic lowering in Wyoming is believed to have occurred during the Eocene (Chase et al., 1998), and the methodology used by Markwick (2007) puts Wyoming 27 % lower in the late Miocene than in the CTRL. A recent study of the Western Cordillera of North America also considers that elevations were generally lower during the late Miocene than today, but argues for considerable evidence of surface uplift during the late Miocene in the westernmost regions north of 45° N (Foster et al., 2010).

D2 Ice sheet configuration

The extent of late Miocene glaciation is much debated (Shackleton and Kennett, 1975; Webb and Harwood, 1991; Wilson, 1995; Pekar and DeConto, 2006; Huybrechts, 1993; Marchant et al., 1996) and perhaps highly variable (Lear et al., 2000). For the late Miocene, the Markwick (2007) reconstruction assumes the East and West Antarctic ice sheets cover the whole Antarctic continent, although ice thickness is generally less than CTRL. The sensitivity experiments of DeConto et al. (2008) and Micheels et al. (2009a) support the evidence for the onset of some glaciation in the Northern Hemisphere during the Miocene (Moran et al., 2006; Kamikuri et al., 2007; Denton and Armstrong, 1969; Thiede and Myhre, 1995, and references therein; Talwani and Udintsev, 1976; Warnke and Hansen, 1977). Markwick (2007) assumes much reduced Northern Hemisphere ice for the late Miocene compared with the extent of the present day Greenland ice sheet. Future work will investigate the impact of ice sheet extent assumptions on the simulated late Miocene climate.

The high latitude topography is lowered in the late Miocene simulations compared to the CTRL, due to the removal of continental ice rather than post-Miocene uplift; Greenland is 60 % lower and Antarctica is very spatially variable, but is on average 4 % lower.

All non-ice covered land grid boxes were initialised with the TRIFFID shrub PFT before the TRIFFID model was switched on, as the simulations were continuations of

pre-existing simulations with global homogenous shrub coverage.

D3 Continental positions

We use the late Miocene land–sea definitions of Markwick (2007), aggregated up to the GCM resolution. Notable changes in continental positions are the more southerly position of the Australian continent, the closed Bering Strait, the extension of Eurasia in to the Arctic, and the open Panama gateway and Indonesian seaway for the late Miocene.

D4 Soil type

Some of the palaeoenvironmental conditions are largely unknown for the Miocene period, such as the soil type which is typically unknown outside of some regions in North America and Kenya (Retallack, 2004; Retallack et al., 1990, 1995, 2002a, b); so for these we use an average homogenous value derived from the CTRL simulation. Soil parameters have been shown to have significant influence on soil hydrology (Osborne et al., 2004), and therefore our choice of soil type could bias the simulated vegetation distribution and modify the simulated climate. Future experiments will be conducted to assess the extent to which the soil type could affect the results presented here.

D5 Bathymetry

Late Miocene palaeobathymetry is assumed to be the same as for the CTRL, except for the land–sea mask itself, which results in a wider Indonesian seaway and an open Panama gateway. The algorithm used to generate the late Miocene bathymetry assumes that the depth of all late Miocene ocean grid boxes (that would be land today in the CTRL simulation) is the average of all neighbouring ocean grid boxes.

As palaeomagnetic studies for plate tectonic reconstruction are difficult to apply to the Indonesian islands (Gourlan et al., 2008), the evolution of their palaeogeography remains uncertain. It is generally believed that the restriction of the Indonesian seaway has occurred in the past 20 Ma, with timing estimates for different water mass restrictions from early Miocene to early late Miocene (van Andel et al., 1975; Edwards, 1975), or even Pliocene (Kennett et al., 1985; Cane and Molnar, 2001; Srinivasan and Sinha, 1998). The late Miocene seaway in our simulations is > 2000 m at its deepest, as for the CTRL.

The closure of the Panama gateway in the Pliocene is the most recent major modification to oceanic gateways (Keigwin, 1982; Duque-Caro, 1990). The shoaling of the region is believed to have commenced in the middle Miocene (Keller and Barron, 1983; Duque-Caro, 1990; Droxler et al., 1998), but determining potential depth of the sill during the late Miocene is problematic; a depth of 200–500 m at 6 Ma is suggested by Collins et al. (1996) and < 100 m depth by the early Pliocene by Keigwin (1982). Duque-Caro (1990) suggests that in the earliest late Miocene, sill depth was ~ 1000 m, and 150–500 m between 8.6–7 Ma, < 150 m at 7–6.3 Ma and < 50 m at the latest Miocene. Given our large timeslab, possible sill depths for the late Miocene range from 1000 m to < 50 m; our bathymetric algorithm produces a depth of 995 m, which lies within the range of estimates.

The choice of bathymetry has been shown to have large regional impacts (e.g. the Greenland–Scotland Ridge, Robinson et al., 2011), but the uncertainty associated with palaeobathymetric reconstruction is large; therefore, future work will seek to assess the climatic uncertainty associated with the choice of palaeobathymetry through climate sensitivity studies.

Supplementary material related to this article is available online at: http://www.clim-past.net/8/1257/2012/cp-8-1257-2012-supplement.zip.

Acknowledgements. This work was carried out using the computing facilities of the Advanced Computing Research Centre at the University of Bristol, http://www.bris.ac.uk/acrc. Catherine Bradshaw is funded by a NERC PhD studentship. Dan Lunt is funded by RCUK. Matthew Pound is funded by the Natural Environment Research Council (UK) and the British Geological Survey University Funding Initiative (PhD studentship NE/G523563/1). We thank the two reviewers and Gregor Knorr for their comments on an earlier version of this manuscript.

Edited by: A. Sluijs

References

Bailey, I. and Sinnott, E.: A botanical index of Cretaceous and Tertiary climates, Science, 41, 831–834, 1915.

Behrensmeyer, A. K., Kidwell, S. M., and Gastaldo, R. A.: Taphonomy and paleobiology, Paleobiology, 26, 103–147, doi:10.1666/0094-8373(2000)26[103:tap]2.0.co;2, 2000.

Bernor R. L., Mittmann H.-W., and Rögl F.: Systematics and Chronology of the Götzendorf "Hipparion" (Late Miocene, Pannonian F, Vienna Basin), Ann. Naturhist. Mus. Wien, 95, 101–120, 1993.

Betts, R. A., Cox, P. M., Collins, M., Harris, P. P., Huntingford, C., and Jones, C. D.: The role of ecosystem-atmosphere interactions in simulated Amazonian precipitation decrease and forest dieback under global climate warming, Theor. Appl. Climatol., 78, 157–175, doi:10.1007/s00704-004-0050-y, 2004.

Bohme, M., Ilg, A., and Winklhofer, M.: late Miocene "washhouse" climate in Europe, Earth Planet. Sc. Lett., 275, 393–401, doi:10.1016/j.epsl.2008.09.011, 2008.

Brandefelt, J. and Otto-Bliesner, B. L.: Equilibration and variability in a last glacial maximum climate simulation with CCSM3, Geophyis. Res. Lett., 36, L19712, doi:10.1029/2009GL040364, 2009.

Bradshaw, C. D., Flecker, R., Ravelo, A. C., Lunt, D., Galaasen, E. V., Spero, H., and Williams, M.: Paleoceanographic model-data comparisons: what exactly are we doing? A case study from the late Miocene, Paleoceanography, in preparation, 2012.

Bruch, A. A., Uhl, D., and Mosbrugger, V.: Miocene climate in Europe – Patterns and evolution – A first synthesis of NECLIME, Palaeogeogr. Palaeocl., 253, 1–7, doi:10.1016/j.palaeo.2007.03.030, 2007.

Bruch, A. A., Utescher, T., Mosbrugger, V., and NECLIME members: Precipitation pat-terns in the Miocene of Central Europe and the development of continentality, Palaeogeogr. Palaeocl., 304, 202–211, 2011.

Cane, M. A. and Molnar, P.: Closing of the Indonesian seaway as a precursor to east African aridircation around 3–4 million years ago, Nature, 411, 157–162, 2001.

Chase, C. G., Gregory-Wodzicki, K. M., Parrish-Jones, J. T., and DeCelles, P. G.: Topographic history of the western Cordillera of North America and controls on climate, in: Tectonic boundary conditions for climate model simulations, edited by: Crowley, T. J. and Burke, K., Oxford Monographs on Geology and Geophysics, Oxford University Press, Oxford UK, 39, 73–99, 1998.

CIESIN (Center for International Earth Science Information Network): Global Rural-Urban Mapping Project (GRUMP) Alpha Version: Urban Extents http://sedac.ciesin.columbia.edu/gpw, 2004

Clark, M. K., House, M. A., Royden, L. H., Whipple, K. X., Burchfiel, B. C., Zhang, X., and Tang, W.: Late Cenozoic uplift of southeastern Tibet, Geology, 33, 525–528, doi:10.1130/G21265.1, 2005.

Collins, L. S., Coates, A. G., Berggren, W. A., Aubry, M. P., and Zhang, J. J.: The late Miocene Panama isthmian strait, Geology, 24, 687–690, 1996.

Cox, P.: Description on the TRIFFID Dynamic Global Vegetation Model, 2001.

Cox, P. M., Betts, R. A., Jones, C. D., Spall, S. A., and Totterdell, I. J.: Acceleration of global warming due to carbon-cycle feedbacks in a coupled climate model, Nature, 408, 184–187, 2000.

Crowley, T. J., and Baum, S. K.: Reconciling Late Ordovician (440 Ma) glaciation with very high (14X) CO_2 levels, J. Geophys. Res., 100, 1093–1101, doi:10.1029/94jd02521, 1995.

Currie, B. S., Rowley, D. B., and Tabor, N. J.: Middle Miocene paleoaltimetry of southern Tibet: Implications for the role of mantle thickening and delamination in the Himalayan orogen, Geology, 33, 181–184, 2005.

DeCelles, P. G., Kapp, P., Ding, L., and Gehrels, G. E.: Late Cretaceous to middle Tertiary basin evolution in the central Tibetan Plateau: Changing environments in response to tectonic partitioning, aridification, and regional elevation gain, Geol. Soc. Am. Bull., 119, 654–680, doi:10.1130/b26074.1, 2007.

DeConto, R. M., Pollard, D., Wilson, P. A., Palike, H., Lear, C. H., and Pagani, M.: Thresholds for Cenozoic bipolar glaciation, Nature, 455, 652-U652, doi:10.1038/Nature07337, 2008.

Demicco, R. V., Lowenstein, T. K., and Hardie, L. A.: Atmospheric pCO(2) since 60 Ma from records of seawater pH, calcium, and primary carbonate mineralogy, Geology, 31, 793–796, 2003.

Denk, T., Grimsson, F., and Kvacek, Z.: The Miocene floras of Iceland and their significance for late Cainozoic North Atlantic biogeography, Bot. J. Linn. Soc., 149, 369–417, 2005.

Denton, G. H. and Armstrong, R. L.: Miocene-Pliocene Glaciations in Southern Alaska, Am. J. Sci., 267, 1121–1142, 1969.

Droxler, A. W., Burke, K., Cunningham, A. D., Hine, A. C., Rosencrantz, D., and Duncan, D.: Caribbean constraints on circulation between Atlantic and Pacific oceans over the past 40 million years, in: Tectonic Boundary Conditions for Climate Reconstruction, edited by: Crowley, T. J. and Burke, K. C., Oxford Monographs Geology and Geophysics, 169–191, 1998.

Duque-Caro, H.: Neogene stratigraphy, paleocenography and paleobiogeography in northwest South-America and the evolution of the Panama Seaway, Palaeogeogr. Palaeocl., 77, 203–234, 1990.

Duringer, P., Schuster, M., Genise, J. F., Mackaye, H. T., Vignaud, P., and Brunet, M.: New termite trace fossils: Galleries, nests and fungus combs from the Chad basin of Africa (Upper Miocene-Lower Pliocene), Palaeogeogr. Palaeocl., 251, 323–353, doi:10.1016/j.palaeo.2007.03.029, 2007.

Edwards, A. R.: Southwest Pacific Cenozoic paleogeography and an integrated Neogene paleocirculation model, Initial. Rep. Deep Sea, 30, 667–684, 1975.

Edwards, J. M. and Slingo, A.: Studies with a flexible new radiation code 1, Choosing a configuration for a large-scale model, Q. J. Roy. Meteor. Soc., 122, 689-719, 1996.

Ehlers, T. A. and Poulsen, C. J.: Large paleoclimate influence the interpretation of Andean Plateau paleoaltimetry, Earth Planet. Sci. Lett., 281, 238–248, 2009.

England, P. and Searle, M. P.: The Cretaceous-Tertiary deformation of the Lhasa Block and its implications for crustal thickening in Tibet, Tectonics, 5, 1–14, 1986.

Eronen, J. T., Ataabadia, M. M., Micheelsb, A., Karme, A., Bernor, R. L., and Fortelius, M.: Distribution history and climatic controls of the late Miocene Pikermian chronofauna, P. Natl. Acad. Sci. USA, 106, 11867–11871, doi:10.1073/pnas.0902598106, 2009.

Eronen, J. T., Puolamäki, K., Liu, L., Lintulaakso, K., Damuth, J., Janis, C., and Fortelius, M.: Precipitation and large herbivorous mammals, Part II: Application to fossil data, Evol. Ecol. Res., 12, 235–248, 2010.

Eronen, J. T., Micheels, A., and Utescher, T.: Comparison of estimates for Mean Annual Precipitation from different proxies, A Pilot Study for European Neogene, Evolutionary Ecology Research, available at: http://www.evolutionary-ecology.com/forthcoming.html, 2012.

Essery, R. and Clark, D. B.: Developments in the MOSES 2 land-surface model for PILPS 2e, Global Planet. Change, 38, 161–164, doi:10.1016/S0921-8181(03)00026-2, 2003.

Etheridge, D. M., Steele, L. P., Langenfelds, R. L., Francey, R. J., Barnola, J. M., and Morgan, V. I.: Natural and anthropogenic changes in atmospheric CO_2 over the last 1000 years from air in Antarctic ice and firn, J Geophys. Res.-Atmos., 101, 4115–4128, 1996.

Fang, X. M., Yan, M. D., Van der Voo, R., Rea, D. K., Song, C. H., Pares, J. M., Gao, J. P., Nie, J. S., and Dai, S.: Late Cenozoic deformation and uplift of the NE Tibetan plateau: Evidence from high-resolution magneto stratigraphy of the Guide Basin, Qinghai Province, China, Geol. Soc. Am. Bull., 117, 1208–1225, doi:10.1130/B25727.1, 2005.

Fauquette, S., Guiot, J., and Suc, J.-P.: A method for climatic reconstruction of the Mediterranean Pliocene using pollen data, Palaeogeogr. Palaeocl., 144, 183–201,

doi:10.1016/S0031-0182(98)00083-2, 1998

Farrera, I., Harrison, S. P., Prentice, I. C., Ramstein, G., Guiot, J., Bartlein, P. J., Bonnefille, R., Bush, M., Cramer, W., von Grafenstein, U., Holmgren, K., Hooghiemstra, H., Hope, G., Jolly, D., Lauritzen, S.-E., Ono, Y., Pinot, S., Stute, M., and Yu, G.: Tropical climates at the Last Glacial Maximum: a new synthesis of terrestrial palaeoclimate data, I: Vegetation, lake-levels and geochemistry, Clim. Dynam., 15, 823–856, 1999.

Fauquette, S., Suc, J.-P., Bertini, A., Popescu, S.-M., Warny, S., Bachiri Taoufiq, N., Perez Villa, M.-J., Chikhi, H., Feddi, N., Subally, D., Clauzon, G., and Ferrier, J.: How much did climate force the Messinian salinity crisis?, Quantified climatic conditions from pollen records in the Mediterranean region, Palaeogeogr. Palaeocl., 238, 281–301, doi:10.1016/j.palaeo.2006.03.029, 2006.

Fluteau, F., Ramstein, G., and Besse, J.: Simulating the evolution of the Asian and African monsoons during the past 30 Myr using an atmospheric general circulation model, J. Geophys. Res.-Atmos., 104, 11995–12018, 1999.

Fortelius, M.: Neogene of the Old World Database of Fossil Mammals (NOW), University of Helsinki, http://www.helsinki.fi/science/now/, 2012.

Foster, G. L., Lunt, D. J., and Parrish, R. R.: Mountain uplift and the glaciation of North America – a sensitivity study, Clim. Past, 6, 707–717, doi:10.5194/cp-6-707-2010, 2010.

Freeman, K. H. and Hayes, J. M.: Fractionation of carbon isotopes by phytoplankton and estimates of ancient CO_2 levels, Global Biogeochem. Cy., 6, 185–198, 1992.

Galeotti, S., von der Heydt, A., Huber, M., Bice, D., Dijkstra, H., Jilbert, T., Lanci, L., and Reichart, G.-J.: Evidence for active El Niño Southern Oscillation variability in the Late Miocene greenhouse climate, Geology, 38, 419–422, doi:10.1130/G30629.1, 2010.

Garzione, C. N., Dettman, D. L., Quade, J., DeCelles, P. G., and Butler, R. F.: High times on the Tibetan Plateau: Paleoelevation of the Thakkhola graben, Nepal, Geology, 28, 339–342, 2000.

Garzione, C. N., Hoke, G. D., Libarkin, J. C., Withers, S., MacFadden, B., Eiler, J., Ghosh, P., and Mulch, A.: Rise of the Andes, Science, 320, 1304–1307, doi:10.1126/science.1148615, 2008.

Gent, P. R. and McWilliams, J. C.: Isopyncnal mixing in ocean circulation models, J. Phys. Oceanogr., 20, 150–155, 1990.

Gladstone, G., Flecker, R., Valdes, P., Lunt, D., and Markwick, P.: The Mediterranean hydrologic budget from a Late Miocene global climate simulation, Palaeogeogr. Palaeocl., 251, 254–267, 2007.

Gordon, C., Cooper, C., Senior, C. A., Banks, H., Gregory, J. M., Johns, T. C., Mitchell, J. F. B., and Wood, R. A.: The simulation of SST, sea ice extents and ocean heat transports in a version of the Hadley Centre coupled model without flux adjustments, Clim. Dynam., 16, 147–168, 2000.

Gourlan, A. T., Meynadier, L. M., and Allègre, C. J.: Tectonically driven changes in the Indian Ocean circulation over the last 25 Ma: Neodymium isotope evidence, Earth Planet. Sci. Lett., 267, 353–364, 2008.

Gradstein, F. M., Ogg, J. G., Smith, A. G., Bleeker, W., Lourens, L. J.: A new Geological Time Scale, with special reference to Precambrian and Neogene, Episodes, 27, 83–100, 2004.

Gregory-Wodzicki, K. M.: Andean paleoelevation estimates: A review and critique, Geol. Soc. Am. Bull., 112, 1091–1105, 2000.

Gregory-Wodzicki, K. M.: A late Miocene subtropical-dry flora from the northern Altiplano, Bolivia, Palaeogeogr. Palaeocl., 180, 331–348, 2002.

Gregory, D. and Rowntree, P. R.: A mass flux convection scheme with representation of cloud ensemble characteristics and stability-dependent closure, Mon. Weather Rev., 118, 1483–1506, 1990.

Harrison, T. M., Copeland, P., Kidd, W. S. F., and Yin, A.: Raising Tibet, Science, 255, 1663–1670, 1992.

Haxeltine, A. and Prentice, I. C.: BIOME3: An equilibrium terrestrial biosphere model based on ecophysiological constraints, resource availability, and competition among plant functional types, Global Biogeochem. Cy., 10, 693–709, 1996.

Henrot, A.-J., François, L., Favre, E., Butzin, M., Ouberdous, M., and Munhoven, G.: Effects of CO_2, continental distribution, topography and vegetation changes on the climate at the Middle Miocene: a model study, Clim. Past, 6, 675–694, doi:10.5194/cp-6-675-2010, 2010.

Hilgen, F., Aziz, H. A., Bice, D., Iaccarino, S., Krijgsman, W., Kuiper, K., Montanari, A., Raffi, I., Turco4, E., and Zachariasse, W.-J.: The Global boundary Stratotype Section and Point (GSSP) of the Tortonian Stage (Upper Miocene) at Monte Dei Corvi, Episodes, 28, 6–17, 2005.

Holdridge, L. R.: Determination of world formations from simple climatic data, Science, 105, 367–368, 1947.

Hughes, J. K., Valdes, P. J., and Betts, R. A.: Dynamical properties of the TRIFFID dynamic global vegetation model, 2004.

Huybrechts, P.: Glaciological modeling of the late Cenozoic East Antarctic ice sheet: stability or dynamism?, Geogr. Anal., 75, 221–238, 1993.

IPCC: Climate Change 2007 – The Physical Science Basis, in: Contribution of Working Group I to the Fourth Assessment Report of the Intergovernmental Panel on Climate Change, 2007 edited by: Solomon, S., Qin, D., Manning, M., Chen, Z., Marquis, M., Averyt, K. B., Tignor, M., and Miller, H. L., Cambridge University Press, Cambridge, 2007.

Jacobs, B. F. and Deino, A. L.: Test of climate-leaf physiognomy regression models, their application to two Miocene floras from Kenya, and Ar-40/Ar-39 dating of the late Miocene Kapturo site, Palaeogeogr. Palaeocl., 123, 259–271, 1996.

Jimenez-Moreno, G., Fauquette, S., and Suc, J. P.: Vegetation, climate and palaeoaltitude reconstructions of the Eastern Alps during the Miocene based on pollen records from Austria, Central Europe, J. Biogeogr., 35, 1638–1649, doi:10.1111/j.1365-2699.2008.01911.x, 2008.

Jones, C.: A fast ocean GCM without flux adjustments, J. Atmos. Ocean. Tech., 20, 1857–1868, 2003.

Kameo, K. and Sato, T.: Biogeography of Neogene calcareous nannofossils in the Caribbean and the eastern equatorial Pacific – floral response to the emergence of the Isthmus of Panama, Mar. Micropaleontol., 39, 201–218, 2000.

Kamikuri, S.-i., Nishi, H., and Motoyama, I.: Effects of late Neogene climatic cooling on North Pacific radiolarian assemblages and oceanographic conditions, Palaeogeogr. Palaeocl., 249, 370–392, 2007.

Kaplan, J. O.: Geophysical Applications of Vegetation Modeling, Ph.D. Thesis, Lund University, Lund, 2001.

Kaplan, J. O., Bigelow, N. H., Bartlein, P. J., Christensen, T. R., Cramer, W., Harrison, S. P., Matveyeva, N. V., McGuire, A. D.,

Murray, D. F., Prentice, I. C., Razzhivin, V. Y., Smith, B. and Walker, D. A., Anderson, P. M., Andreev, A. A., Brubaker, L. B., Edwards, M. E., Lozhkin, A. V. and Ritchie, J.: Climate change and Arctic ecosystems II: Modeling, palaeodata-model comparisons, and future projections, J. Geophys. Res.-Atmos., 108, 8171, doi:10.1029/2002JD002559, 2003.

Keigwin, L.: Isotopic paleoceanography of the Caribbean and East Pacific: role of Panama uplift in late Neogene time, Science, 217, 350–353, 1982.

Keller, G. and Barron, J. A.: Paleoceanographic Implications of Miocene Deep-Sea Hiatuses, Geol. Soc. Am. Bull., 94, 590–613, 1983.

Kennett, J. P., Keller, G., and Srinivasan, M. S.: Miocene Planktonic Foraminiferal Biogeography and Paleoceanographic Development of the Indo-Pacific Region, Geol. Soc. Am. Mem., 163, 197–236, 1985.

Kingston, J. D. and Hill, A.: late Miocene palaeoenvironments in Arabia: A synthesis., in: Fossil vertebrates of Arabia, edited by: Whybrow, P. J. and Hill, A., Yale University Press, 1999.

Knorr, G., Butzin, M., Micheels, A., and Lohmann, G.: A warm Miocene climate at low atmospheric CO_2 levels, Geophys. Res. Lett., 38, L20701, doi:10.1029/2011gl048873, 2011.

Krapp, M. and Jungclaus, J. H.: The Middle Miocene climate as modelled in an atmosphere-ocean-biosphere model, Clim. Past, 7, 1169–1188, doi:10.5194/cp-7-1169-2011, 2011.

Kuhlemann, J.: Paleogeographic and paleotopographic evolution of the Swiss and Eastern Alps since the Oligocene, Global Planet. Change, 58, 224–236, doi:10.1016/j.gloplacha.2007.03.007, 2007.

Kürschner, W. M., vanderBurgh, J., Visscher, H., and Dilcher, D. L.: Oak leaves as biosensors of late Neogene and early Pleistocene paleoatmospheric CO_2 concentrations, Mar. Micropaleontol., 27, 299–312, 1996.

Kürschner, W. M., Kvacek, Z., and Dilcher, D. L.: The impact of Miocene atmospheric carbon dioxide fluctuations on climate and the evolution of terrestrial ecosystems, P. Natl. Acad. Sci. USA, 105, 449–453, doi:10.1073/pnas.0708588105, 2008.

Kutzbach, J. E. and Behling, P.: Comparison of simulated changes of climate in Asia for two scenarios: Early Miocene to present, and present to future enhanced greenhouse, Global Planet. Change, 41, 157–165, doi:10.1016/j.gloplacha.2004.01.015, 2004.

Lear, C. H., Elderfield, H., and Wilson, P. A.: Cenozoic deep-sea temperatures and global ice volumes from Mg/Ca in benthic foraminiferal calcite, Science, 287, 269–272, 2000.

Lewis, A. R., Marchant, D. R., Ashworth, A. C., Hedenas, L., Hemming, S. R., Johnson, J. V., Leng, M. J., Machlus, M. L., Newton, A. E., Raine, J. I., Willenbring, J. K., Williams, M., and Wolfe, A. P.: Mid-Miocene cooling and the extinction of tundra in continental Antarctica, P. Natl. Acad. Sci. USA, 105, 10676–10680, doi:10.1073/pnas.0802501105, 2008.

Lohmann, G., Butzin, M., Micheels, A., Bickert, T., and Mosbrugger, V.: Effect of vegetation on the Late Miocene ocean circulation, Clim. Past Discuss., 2, 605–631, doi:10.5194/cpd-2-605-2006, 2006.

Loveland, T. R. and Belward, A. S.: The IGBP-DIS global 1 km land cover data set, DISCover: First results, Int. J. Remote Sens., 18, 3289–3295, 1997.

Lunt, D. J., de Noblet-Ducoudre, N., and Charbit, S.: Effects of a melted Greenland ice sheet on climate, vegetation, and the cryosphere., Clim. Dynam., 23, 679–694, 2004.

Lunt, D. J., Ross, I., Hopley, P. J., and Valdes, P. J.: Modelling late Oligocene C-4 grasses and climate, Palaeogeogr. Palaeocl., 251, 239–253, doi:10.1016/j.palaeo.2007.04.004, 2007.

Lunt, D. J., Flecker, R., Valdes, P. J., Salzmann, U., Gladstone, R., and Haywood, A. M.: A methodology for targeting palaeo proxy data acquisition: A case study for the terrestrial late Miocene, Earth Planet. Sci. Lett., 271, 53–62, doi:10.1016/j.epsl.2008.03.035, 2008a.

Lunt, D. J., Valdes, P. J., Haywood, A., and Rutt, I. C.: Closure of the Panama Seaway during the Pliocene: implications for climate and Northern Hemisphere glaciation, Clim. Dynam., 30, 1–18, doi:10.1007/s00382-007-0265-6, 2008b.

Lunt, D. J., Flecker, R., and Clift, P. D.: The impacts of Tibetan uplift on palaeoclimate proxies, J. Geol. Soc. London, Special Publications, 342, 279–291, 2010.

Marchant, D. R., Denton, G. H., Swisher, C. C., and Potter, N.: Late Cenozoic Antarctic paleoclimate reconstructed from volcanic ashes in the Dry Valleys region of southern Victoria Land, Geol. Soc. Am. Bull., 108, 181–194, 1996.

Markwick, P. J.: The palaeogeographic and palaeoclimatic significance of climate proxies for data-model comparisons, Deep-Time Perspectives on Climate Change: Marrying the Signal from Computer Models and Biological Proxies, 251–312, 2007.

Markwick, P. J. and Valdes, P. J.: Palaeo-digital elevation models for use as boundary conditions in coupled ocean-atmo sphere GCM experiments: a Maastrichtian (late Cretaceous) example, Palaeogeogr. Palaeocl., 213, 37–63, doi:10.1016/j.palaeo.2004.06.015, 2004.

Martin, R. E.: Taphonomy. A Process Approach, Cambridge University Press, Cambridge, 508 pp., 1999.

Matthews, E.: Global vegetation and land use: New high-resolution data bases for climate studies, J. Clim. Appl. Meteorol., 22, 474–487, 1983.

McGowran, B., Holdgate, G. R., Li, Q., and Gallagher, S. J.: Cenozoic stratigraphic succession in southeastern Australia, Aust. J. Earth Sci., 51, 459–496, 2004.

Meehl, G. A., Covey, C., Taylor, K. E., Delworth, T., Stouffer, R. J., Latif, M., McAvaney, B., and Mitchell, J. F. B.: The WCRP CMIP3 multimodel dataset: a new era in climate change research, B. Am. Meterol. Soc., 88, 1383–1394, 2007.

Micheels, A., Bruch, A. A., Uhl, D., Utescher, T., and Mosbrugger, V.: A late Miocene climate model simulation with ECHAM4/ML and its quantitative validation with terrestrial proxy data, Palaeogeogr. Palaeocl., 253, 251–270, doi:10.1016/j.palaeo.2007.03.042, 2007.

Micheels, A., Bruch, A., and Mosbrugger, V.: Miocene Climate Modelling Sensitivity Experiments for Different CO2 Concentrations, Palaeontol. Electron., 12, Artno. 12.2.5A, 2009a.

Micheels, A., Eronen, J., and Mosbrugger, V.: The late Miocene climate response to a modern Sahara desert, Global Planet. Change, 67, 193–204, doi:10.1016/j.gloplacha.2009.02.005, 2009b.

Micheels, A., Bruch, A. A., Eronen, J., Fortelius, M., Harzhauser, M., Utescher, T., and Mosbrugger, V.: Analysis of heat transport mechanisms from a late Miocene model experiment with a fully-coupled atmosphere-ocean general circulation model, Palaeogeogr. Palaeocl., 304, 337–350 2011.

Mitchell, T. D. and Jones, P. D.: An improved method of constructing a database of monthly climate observations and associated high-resolution grids, Int. J. Climatol., 25, 693–712, 2005.

Molnar, P., England, P., and Martinod, J.: Mantle Dynamics, Uplift of the Tibetan Plateau, and the Indian Monsoon, Rev. Geophys., 31, 357–396, 1993.

Montuire, S., Maridet, O., and Legendre, S.: late Miocene-Early Pliocene temperature estimates in Europe using rodents, Palaeogeogr. Palaeocl., 238, 247–262, doi:10.1016/j.palaeo.2006.03.026, 2006.

Moran, K., Backman, J., Brinkhuis, H., Clemens, S. C., Cronin, T., Dickens, G. R., Eynaud, F., Gattacceca, J., Jakobsson, M., Jordan, R. W., Kaminski, M., King, J., Koc, N., Krylov, A., Martinez, N., Matthiessen, J., McInroy, D., Moore, T. C., Onodera, J., O'Regan, M., Palike, H., Rea, B., Rio, D., Sakamoto, T., Smith, D. C., Stein, R., St. John, K., Suto, I., Suzuki, N., Takahashi, K., Watanabe, M., Yamamoto, M., Farrell, J., Frank, M., Kubik, P., Jokat, W., and Kristoffersen, Y.: The Cenozoic palaeoenvironment of the Arctic Ocean, Nature, 441, 601–605, doi:10.1038/Nature04800, 2006.

Morgan, P. and Swanberg, C. A.: On the Cenozoic Uplift and Tectonic Stability of the Colorado Plateau, J. Geodyn., 3, 39–63, 1985.

Mosbrugger, V. and Utescher, T.: The coexistence approach – a method for quantitative reconstructions of Tertiary terrestrial palaeoclimate data using plant fossils, Palaeogeogr. Palaeocl., 134, 61–86, doi:10.1016/s0031-0182(96)00154-x, 1997.

Nisancioglu, K. H., Raymo, M. E., and Stone, P. H.: Reorganization of Miocene deep water circulation in response to the shoaling of the Central American Seaway, Paleoceanography, 18, 1006, doi:10.1029/2002pa000767, 2003.

NOAA: Data Announcement 88-MGG-02, Digital relief of the Surface of the Earth, National Geophysical Data Center, Boulder, Colorado, 1988.

Olson, J. S., Watts, J. A., and Allison, L. J.: Carbon in live vegetation of major world ecosystems, Oak Ridge National Laboratory, Oak Ridge, 1983.

Osborne, T. M., Lawrence, D. M., Slingo, J. M., Challinor, A. J., and Wheeler, T. R.: Influence of vegetation on the local climate and hydrology in the Tropics: Sensitivity to soil parameters, Clim. Dynam., 23, 45–61, 2004.

Pagani, M., Arthur, M. A., and Freeman, K. H.: Miocene evolution of atmospheric carbon dioxide, Paleoceanography, 14, 273–292, 1999a.

Pagani, M., Freeman, K. H., and Arthur, M. A.: late Miocene atmospheric CO_2 concentrations and the expansion of C-4 grasses, Science, 285, 876–879, 1999b.

Pearson, P. N. and Palmer, M. R.: Atmospheric carbon dioxide concentrations over the past 60 million years, Nature, 406, 695–699, 2000.

Pekar, S. F. and DeConto, R. M.: High-resolution ice-volume estimates for the early Miocene: Evidence for a dynamic ice sheet in Antarctica, Palaeogeogr. Palaeocl., 231, 101–109, doi:10.1016/j.palaeo.2005.07.027, 2006.

Pound, M. J., Haywood, A. M., Salzmann, U., Riding, J. B., Lunt, D. J., and Hunter, S. J.: A Tortonian (late Miocene, 11.61–7.25 Ma) global vegetation reconstruction, Palaeogeogr. Palaeocl., 300, 29–45, 2011.

Pound, M. J., Haywood, A. M., Salzmann, U., Riding, J. B. Global vegetation dynamics and latitudinal temperature gradients during the mid to Late Miocene (15.97–5.33 Ma), Earth Sci. Rev., 112, 1–22, 2012

Prell, W. L. and Kutzbach, J. E.: Sensitivity of the Indian Monsoon to Forcing Parameters and Implications for Its Evolution, Nature, 360, 647–652, 1992.

Prentice, I. C., Cramer, W., Harrison, S. P., Leemans, R., Monserud, R. A., and Solomon, A. M.: A global biome model based on plant physiology and dominance, soil properties and climate, J. Biogeogr., 19, 117–134, doi:10.2307/2845499, 1992.

Ramankutty, N. and Foley, J. A.: Estimating historical changes in global land cover: Croplands from 1700 to 1992, Global Biogeochem. Cy., 13, 997–1027, 1999.

Ramstein, G., Fluteau, F., Besse, J., and Joussaume, S.: Effect of orogeny, plate motion and land sea distribution on Eurasian climate change over the past 30 million years, Nature, 386, 788–795, 1997.

Retallack, G. J.: A 300-million-year record of atmospheric carbon dioxide from fossil plant cuticles, Nature, 411, 287–290, doi:10.1038/35077041, 2001.

Retallack, G. J.: Late Oligocene bunch grassland and early Miocene sod grassland paleosols from central Oregon, USA, Palaeogeogr. Palaeocl., 207, 203–237, doi:10.1016/j.palaeo.2003.09.027, 2004.

Retallack, G. J., Dugas, D. P., and Bestland, E. A.: Fossil Soils and Grasses of a Middle Miocene East-African Grassland, Science, 247, 1325–1328, 1990.

Retallack, G. J., Bestland, E. A., and Dugas, D. P.: Miocene Paleosols and Habitats of Proconsul on Rusinga Island, Kenya, J. Hum. Evol., 29, 53–91, 1995.

Retallack, G. J., Tanaka, S., and Tate, T.: late Miocene advent of tall grassland paleosols in Oregon, Palaeogeogr. Palaeocl., 183, 329–354, Pii S0031-0182(02)00250-X, 2002a.

Retallack, G. J., Wynn, J. G., Benefit, B. R., and McCrossin, M. L.: Paleosols and paleoenvironments of the middle Miocene, Maboko Formation, Kenya, J. Hum. Evol., 42, 659–703, doi:10.1006/jhev.2002.0553, 2002b.

Robinson, M. M., Valdes, P. J., Haywood, A. M., Dowsett, H. J., Hill, D. J., and Jones, S. M.: Bathymetric controls on Pliocene North Atlantic and Arctic sea surface temperature and deepwater production, Palaeogeogr. Palaeocl., 309, 92–97, doi:10.1016/j.palaeo.2011.01.004, 2011.

Rowley, D. B. and Currie, B. S.: Palaeo-altimetry of the late Eocene to Miocene Lunpola basin, central Tibet, Nature, 439, 677–681, doi:10.1038/Nature04506, 2006.

Rowley, D. B. and Garzione, C. N.: Stable isotope-based paleoaltimetry, Annu. Rev. Earth. Pl. Sc., 35, 463–508, 2007.

Rowley, D. B., Pierrehumbert, R. T., and Currie, B. S.: A new approach to stable isotope-based paleoaltimetry: implications for paleoaltimetry and paleohypsometry of the High Himalaya since the late Miocene, Earth Planet. Sci. Lett., 188, 253–268, 2001.

Ruddiman, W. F., Kutzbach, J. E., and Prentice, I. C.: Testing the climatic effects of orography and CO_2 with general circulation and biome models., Tectonic Uplift and Climate Change, edited by: Ruddiman, W. F., Plenum Publishing Corporation, New York, 1997.

Saggerson, E. P. and Baker, B. H.: Post-Jurassic erosion-surfaces in eastern Kenya and their deformation in relation to rift structure,

Quarterly J. Geol. Soc. London, 121, 51–72, 1965.

Salzmann, U., Haywood, A. M., and Lunt, D. J.: The past is a guide to the future? Comparing Middle Pliocene vegetation with predicted biome distributions for the twenty-first century, Philos. T. R. Soc. A, 367, 189–204, 2009.

Schneider, B. and Schmittner, A.: Simulating the impact of the Panamanian seaway closure on ocean circulation, marine productivity and nutrient cycling, Earth Planet. Sci. Lett., 246, 367–380, 2006.

Schneider, A., Friedl, M. A., and Potere, D.: A new map of global urban extent from MODIS satellite data., Environ. Res. Lett., 4, 044003, doi:10.1088/1748-9326/4/4/044003, 2009.

Seager, R., Battisti, D. S., Yin, J., Naik, N., Gordon, N., Clement, A. C., and Cane, M. A.: Is the Gulf Stream responsible for Europe's mild winters?, Q. J. Roy. Meteor. Soc., 128, 2563–2586, 2002.

Shackleton, N. J. and Kennett, J. P.: Paleotemperature history of the Cenozoic and the initiation of Antarctic glaciation: oxygen and carbon isotope analyses in DSDP Sites 277, 279, and 281, p. 743–755, US Government Printing Office, Washington, 743–755, 1975.

Sjostrom, D. J., Hren, M. T., Horton, T. W., Waldbauer, J. R., and Chamberlain, C. P.: Stable isotopic evidence for a pre-late Miocene elevation gradient in the Great Plains-Rocky Mountain region, USA, Geol. S. Am. S., 398, 309–319, 2006.

Smith, R. N. B.: Experience and developments with the layer cloud and boundary layer mixing schemes in the UK Meterological Office Unified Model, ECMWF/GCSS workshop on parameterisation of the cloud-topped boundary layer, Reading, England, 1993.

Spicer, R. A.: Recent and Future Developments of CLAMP: Building on the Lagacy of Jack A. Wolfe, Cour. For. Senkenbg., 258, 109–118, 2007.

Spicer, R. A., Harris, N. B. W., Widdowson, M., Herman, A. B., Guo, S. X., Valdes, P. J., Wolfe, J. A., and Kelley, S. P.: Constant elevation of southern Tibet over the past 15 million years, Nature, 421, 622–624, doi:10.1038/nature01356, 2003.

Spicer, R. A., Valdes, P. J., Spicer, T. E. V., Craggs, H. J., Srivastava, G., Mehrotra, R. C., and Yang, J.: New Developments in CLAMP: Calibration using global gridded mteorological data., Palaeogeogr. Palaeocl., 283, 91–98, 2009.

Spiegel, C., Kuhlemann, J., Dunkl, I., and Frisch, W.: Paleogeography and catchment evolution in a mobile orogenic belt: the Central Alps in Oligo-Miocene times, Tectonophysics, 341, 33–47, 2001.

Srinivasan, M. S. and Sinha, D. K.: Early Pliocene closing of the Indonesian Seaway: evidence from north-east Indian Ocean and tropical Pacific deep sea cores, J. Asian Earth Sci., 16, 29–44, 1998.

Steininger, F. F.: Chronostratigraphy, Geochronology and Biochronology of the Miocene European Land Mammal Mega-Zones (ELMMZ) and the Miocene Mammal-Zones, In:The Miocene Land Mammals of Europe, edited by: Rössner, G. E. and Heissig, K., Verlag Dr. Friedrich Pfeil, 9–24, 1999.

Steppuhn, A., Micheels, A., Geiger, G., and Mosbrugger, V.: Reconstructing the late Miocene climate and oceanic heat flux using the AGCM ECHAM4 coupled to a mixed–layer ocean model with adjusted flux correction, Palaeogeogr. Palaeocl., 238, 399–423, doi:10.1016/j.palaeo.2006.03.037, 2006.

Steppuhn, A., Micheels, A., Bruch, A. A., Uhl, D., Utescher, T., and Mosbrugger, V.: The sensitivity of ECHAM4/ML to a double CO_2 scenario for the late Miocene and the comparison to terrestrial proxy data, Global Planet. Change, 57, 189–212, doi:10.1016/j.gloplacha.2006.09.003, 2007.

Takahashi, K. and Battisti, D. S.: Processes controlling the mean tropical Pacific Precipitation Pattern: I. The Andes and the Eastern Pacific ITCZ., J. Climate, 20, 3434–3451, 2007.

Talwani, M. and Udintsev, G. (Eds.): in: Initial Reports Deep Sea Drilling Project US Government Printing Office, Washington, DC, 1976.

Texier, D., de Noblet, N., Harrison, S. P., Haxeltine, A., Jolly, D., Joussaume, S., Laarif, F., Prentice, I. C., and Tarasov, P.: Quantifying the role of biosphere-atmosphere feedbacks in climate change: coupled model simulations for 6000 years BP and comparison with palaeodata for northern Eurasia and northern Africa, Clim. Dynam., 13, 865–882, 1997.

Thiede, J. and Myhre, A. M.: Non-steady behaviour in the Cenozoic Polar North atlantic System: The Onset and Variability of Northern Hemisphere Glaciations, Philosophical Transactions: Physical Sciences and Engineering, 352, 373–385, 1995.

Thiel, C., Klotz, S., and Uhl, D.: Palaeoclimate estimates for selected leaf-floras from the Middle Pliocene (Reuverian) of Central Europe based on different palaeobotanical techniques, Turk. J. Earth Sci., 21, 263–287, 2012.

Tonazzio, T., Gregory, J. M., and Huybrechts, P.: Climatic Impact of a Greenland Deglaciation and its Possible Irreversibility', J. Climate, 17, 21–33, 2004.

Tripati, A., Roberts, C., and Eagle, R.: Coupling of CO_2 and ice sheet stability over major climate transitions of the last 20 million years, Science, 326, 1394–1397, 2009.

Truswell, E. M.: Vegetation changes in the Australian tertiary in response to climatic and phytogeographic forcing factors, Aust. Syst. Bot., 6, 533–557, doi:10.1071/sb9930533, 1993.

Uhl, D., Mosbrugger, V., Bruch, A., and Utescher, T.: Reconstructing palaeotemperatures using leaf floras – case studies for a comparison of leaf margin analysis and the coexistence approach, Rev. Palaeobot. Palynology, 126, 49–64, 2003.

Uhl, D., Bruch, A. A., Traiser, C., and Klotz, S.: Palaeoclimate estimates for the Middle Miocene Schrotzburg flora (S-Germany) – a multi-method approach, Int. J. Earth Sci., 95, 1071–1085, 2006.

Uhl, D., Klotz, S., Traiser, C., Thiel, C., Utescher, T., Kowalski, E. A., and Dilcher, D. L.: Paleotemperatures from fossil leaves – a European perspective. Palaeogeogr. Palaeocl., 248, 24–31, 2007.

Utescher, T., Böhme, M., and Mosbrugger, V.: The Neogene of Eurasia: Spatial gradients and temporal trends – The second synthesis of NECLIME, Palaeogeogr. Palaeocl., 304, 196–201, doi:10.1016/j.palaeo.2011.03.012, 2011.

van Andel, T. H., Heath, G. R., and Moore Jr., T. C.: Cenozoic history and paleoceanography of the Central Equatorial Pacific Ocean, Geol. Soc. Am. Mem., 143, 134 pp., 1975.

van Dam, J. A.: Geographic and temporal patterns in the late Neogene (12–3 Ma) aridification of Europe: The use of small mammals paleoprecipitation proxies, Palaeogeogr. Palaeocl., 238, 190–218, doi:10.1016/j.palaeo.2006.03.025, 2006.

Vignaud, P., Duringer, P., Mackaye, H. T., Likius, A., Blondel, C., Boisserie, J. R., de Bonis, L., Eisenmann, V., Etienne, M. E., Geraads, D., Guy, F., Lehmann, T., Lihoreau, F., Lopez-Martinez, N., Mourer-Chauvire, C., Otero, O., Rage, J. C., Schuster, M., Viriot,

L., Zazzo, A., and Brunet, M.: Geology and palaeontology of the Upper Miocene Toros-Menalla hominid locality, Chad, Nature, 418, 152–155, doi:10.1038/Nature00880, 2002.

Warnke, D. A. and Hansen, M. E.: Sediments of glacial origins in the area of DSDP leg 38 (Norwegian Greenland seas): Preliminary results from Sites 336 and 344, Naturforsch. Ges. Freib. Breisgau Ber., 67, 371–392, 1977.

Webb, P. N. and Harwood, D. M.: Late Cenozoic Glacial History of the Ross Embayment, Antarctica, Quaternary Sci. Rev., 10, 215–223, 1991.

Western, D. and Behrensmeyer, A. K.: Bones track community structure over four decades of ecological change, Science, 324, 1061–1064, 2009.

Wilson, T. J.: Cenozoic Transtension Along the Transantarctic Mountains West Antarctic Rift Boundary, Southern Victoria-Land, Antarctica, Tectonics, 14, 531–545, 1995.

Wilson, M. F. and Henderson-Sellers, A.: A global archive of land cover and soils data for use in general-circulation climate models, J. Climatol., 5, 119–143, 1985.

Wolfe, J. A.: A method of obtaining climatic parameters from leaf assemblages., US Geological Survey Bulletin, 2040, 73 pp., 1993.

Wolfe, J. A.: Tertiary climatic changes at middle latitudes of western North America, Palaeogeogr. Palaeocl., 108, 195–205, 1994.

Wolfe, J. A., Schorn, H. E., Forest, C. E., and Molnar, P.: Paleobotanical evidence for high altitudes in Nevada during the Miocene, Science, 276, 1672–1675, 1997.

Worobiec, G. and Lesiak, M. A.: Plant megafossils from the Neogene deposits of Stawek-1A (Belchatow, Middle Poland), Rev. Palaeobot. Palyno., 101, 179–208, 1998.

Yang, J., Spicer, R., Spicer, T., Li, C.-S.: "CLAMP Online": a new web-based palaeoclimate tool and its application to the terrestrial Paleogene and Neogene of North America, Palaeobiodiversity and Palaeoenvironments 91, 163–183, 2011.

Yemane, K., Bonnefille, R., and Faure, H.: Paleoclimatic and Tectonic Implications of Neogene Microflora from the Northwestern Ethiopian Highlands, Nature, 318, 653–656, 1985.

Zhang, Z., Huijun, W., Zhengtang, G., and Dabang, J.: Impacts of tectonic changes on the reorganization of the Cenozoic paleoclimatic patterns in China, Earth Planet. Sci. Lett., 257, 622–634, 2007a.

Zhang, Z., Wang, H., Guo, Z., and Jiang, D.: What triggers the transition of palaeoenvironmental patterns in China, the Tibetan Plateau uplift or the Paratethys Sea retreat?, Palaeogeogr. Palaeocl., 245, 317–331, 2007b.

Zhang, Z., Nisancioglu, K. H., Flatøy, F., Bentsen, M., Bethke, I., and Wang, H.: Tropical seaways played a more important role than high latitude seaways in Cenozoic cooling, Clim. Past, 7, 801–813, doi:10.5194/cp-7-801-2011, 2011.